The Journal of Immunology

Hypoxic Trophoblast HMGB1 Induces Endothelial Cell Hyperpermeability via the TRL-4/Caveolin-1 Pathway

Rongzhen Jiang, Jingjing Cai, Zhaowei Zhu, Dandan Chen, Jiemei Wang, Qingde Wang, Yincheng Teng, Yajuan Huang, Minfang Tao, Aibin Xia, Min Xue, Shenghua Zhou and Alex F. Chen

J Immunol 2014; 193:5000-5012; Prepublished online 22 October 2014;
doi: 10.4049/jimmunol.1303445
http://www.jimmunol.org/content/193/10/5000

The Journal of Immunology is published twice each month by
The American Association of Immunologists, Inc.,
1451 Rockville Pike, Suite 650, Rockville, MD 20852

Print ISSN: 0022-1767 Online ISSN: 1550-6606.

Hypoxic Trophoblast HMGB1 Induces Endothelial Cell Hyperpermeability via the TRL-4/Caveolin-1 Pathway

Rongzhen Jiang,*[,1] Jingjing Cai,[†,1] Zhaowei Zhu,[‡,1] Dandan Chen,[†] Jiemei Wang,[†] Qingde Wang,[†] Yincheng Teng,* Yajuan Huang,* Minfang Tao,* Aibin Xia,[†] Min Xue,[†] Shenghua Zhou,[‡] and Alex F. Chen[†]

High mobility group box 1 (HMGB1) plays an important role in the pathologic processes of endothelial permeability under oxidative stress. Trophoblast oxidative stress has been implicated in the pathophysiology of preeclampsia (PE). HMGB1 serum levels are increased in PE. However, the potential roles of HMGB1 in endothelial permeability in PE remain unclear. We assessed the effects of the hypoxic trophoblast on the permeability of the endothelial monolayer. Our results showed that the hypoxic trophoblast displayed higher HMGB1 mRNA, intracellular HMGB1 protein, and HMGB1 in conditioned medium than those of the normoxic trophoblast did. The hypoxic trophoblast conditioned medium increased the endothelial monolayer permeability and increased TLR 4 and caveolin-1 (CAV-1) protein expression in endothelial cells, which was inhibited by glycyrrhizic acid and HMGB1 small interfering RNA transfection to trophoblasts before hypoxia. The increased endothelial permeability induced by hypoxic trophoblast conditioned medium could be inhibited with TLR4 or CAV-1 gene silencing in endothelial cells. Immunoprecipitation showed that CAV-1 and TLR4 are colocalized in HUVECs and C57BL/6 mouse kidney. TLR4 small interfering RNA suppressed CAV-1 protein expression in endothelial cells upon stimulation of hypoxic trophoblast conditioned medium or HMGB1. We conclude that hypoxic trophoblasts play an important role in the mechanism of general edema (including protein urine) in PE via increasing endothelial monolayer permeability through the HMGB1/TLR4/CAV-1 pathway. ***The Journal of Immunology*****, 2014, 193: 5000–5012.**

High mobility group box 1 (HMGB1) is a ubiquitously expressed, DNA-binding nuclear protein involved in the stabilization of nucleosomes. HMGB1 is actively released after cytokine stimulation and metabolic stress, such as hypoxia (1); it is also released passively during cell death (2). The importance of HMGB1 as a proinflammatory cytokine has been shown in diseases of chronic inflammation and exaggerated immune responses, such as atherosclerosis (3), sepsis (4), and ischemia-induced angiogenesis (5). HMGB1 does not initiate an acute inflammatory course. Instead, it mediates a chronic process leading to cellular dysfunction and tissue destruction. It has been recently established that HMGB1 increases endothelial monolayer permeability, which leads to protein-rich edema (6, 7); however, the underlying mechanisms are not clear yet.

Preeclampsia (PE) is an oxidative stress process in the placenta leading to hypertension, proteinuria, edema, endothelial cell dysfunction, and placenta atherosclerosis (8). Placental hypoxia can cause trophoblast necrosis and apoptosis (9). Postischemic inflammation is an essential step in the progression of endothelial cell injury in PE (8). A recent study showed that HMGB1 serum levels are increased in severe PE, most notably in patients experiencing early-onset PE (10). General edema and high urine protein are the main characteristics of early-onset PE. It is reported that HMGB1 increases endothelial cell permeability in sepsis and cerebral ischemic pathogenesis by activation of pattern recognition receptors, TLR4, TLR2, and the receptor for advanced glycation endproducts (RAGE) (11, 12). High endothelial cell permeability is the main cause of general edema and high urine protein in PE (8); however, the underlying pathogenic relationship between HMGB1 and endothelial cell dysfunction in PE remains unexplored.

Increased endothelial permeability in the kidney is also a hallmark of endothelial dysfunction in PE. Studies have shown that increased endothelial permeability is associated with the phosphorylation of endothelial specific-junction protein, vascular endothelial–cadherin (VE-cadherin), and an altered distribution of VE-cadherin at endothelial junctions (13). Moreover, caveolin-1 (CAV-1), a structural and scaffold protein required for caveolae formation and transcellular transport, also plays an important role in oxidative stress–induced paracellular hyperpermeability, inflammation-evoked pulmonary vascular hyperpermeability, and protein-rich edema formation (14). A recent study also demon-

*Department of Obstetrics and Gynecology, Shanghai Jiaotong University No. 6 People's Hospital, Shanghai 200233, China; [†]Center for Vascular and Translational Medicine, the College of Pharmacy, and The Third Xiangya Hospital, Central South University, Changsha, Hunan 410013, China; [‡]Department of Cardiology, The Second Xiangya Hospital, Central South University, Changsha, Hunan 410011, China

[1]R.J., J.C., and Z.Z. share first authorship.

Received for publication January 16, 2014. Accepted for publication September 16, 2014.

This work was supported in part by National Basic Research Program of China (973 Program) Grant 2014CB542400; National Science Foundation of China Projects 81130004, 81370359, and 913392019 (to A.F.C.), 31101065 (to R.J.), and 81200236 (to J.C.); and Shanghai Science and Technology Commission Project 10411966500 (to Y.T.).

Address correspondence and reprint requests to Dr. Alex F. Chen, The Third Xiangya Hospital and the College of Pharmacy, Central South University, 138 Tong Zi Bo Road, Changsha, Hunan 410013 China. E-mail address: afychen@yahoo.com

Abbreviations used in this article: CAV-1, caveolin-1; CM, conditioned medium; DiI-Ac-LDL, 1,1′-dioctadecyl-1,3,3,3′,3′-tetramethyl-indocarbocyanine-acetylated low-density lipoprotein; EC, endothelial cell; EGM-2, endothelial cell growth media; GA, glycyrrhizic acid; HMGB1, high mobility group box 1; JC1, 5,5′,6,6′-tetrachloro-1,1′,3,3′-tetraethylbenzimidazolylcarbocyanine iodide; MAEC, mouse arterial endothelial cell; MTT, 3-(4,5-dimethylthiazol-2-yl)-2,5-diphenyltetrazolium bromide; PE, preeclampsia; PI, propidium iodide; PMT, primary mouse trophoblast; RAGE, receptor for advanced glycation end products; rHMGB1, recombinant HMGB1; siRNA, small interfering RNA; VE-cadherin, vascular endothelial–cadherin; VWF-VII, von Willebrand factor-VII.

strated that CAV-1 is an important mechanism mediating oxidant-induced vascular hyperpermeability (15, 16). However, the underlying regulating pathway of kidney endothelial barrier dysfunction in PE is still unknown.

JEG-3 cell line derived from the placenta tissue of choriocarcinoma and have features of both cytotrophoblasts and extravillous trophoblasts. Because of the expression of human chorionic gonadotrophin (hCG), MHC, class I, G (HLA-G), cytokeratin 7, human chorionic somatomammotropin (placental lactogen), and progesterone, JEG-3 cell line is recommended for regulation studies of both trophoblast migration and invasion properties as well as trophoblast proliferation (17, 18).

Based on these considerations, the current study was designed to answer several questions, such as whether hypoxic JEG-3 cells and primary mouse trophoblasts (PMTs) release the "danger signal" HMGB1, whether hypoxic trophoblast (including JEG-3 cells and PMTs) conditioned medium (CM) increases the permeability of the endothelial cell monolayer, and whether hypoxic JEG-3 and PMT CM stimulation of endothelial monolayer permeability involves CAV-1 pathways. We also aimed to detect whether increased endothelial cell permeability is HMGB1-TLR/RAGE-CAV-1 pathway dependent. Glycyrrhizic acid (GA), the main logic activities such as antioxidative, anti-inflammatory, antiulcerous, antidotal, antiallergic, antiviral, immunomodulating, hepatoprotective, and cardioprotective properties (19–22). It was demonstrated that GA played an important role in the inhibition of HMGB1 (23, 24); therefore, we also aimed to evaluate the effect of GA as an inhibitor of hypoxia trophoblast (including PMT and JEG-3) HMGB1 induced hyperpermeability of endothelial cells (ECs), including HUVECs and mouse arterial endothelial cells [MAECs].

Materials and Methods

Animals

Wild type C57BL/6, CAV-1$^{-/-}$ (C57BL/6J background) male and female mice (8–12 wk of age) were obtained from Jackson Laboratories; TLR4 $^{-/-}$ mice (C57BL/6J background) were provided by Dr. T. Billiar (University of Pittsburgh Medical Center, Pittsburgh, PA). Mice were sacrificed to obtain PMTs and mouse arterial endothelial cells (MAECs) on day 11 of gestation. All the mice used had identical genetic backgrounds. All animal procedures were performed according to Institutional Animal Care and Use Committee guidelines.

PMTs isolation from wild type C57BL/6 pregnant mice

First-trimester PMTs were isolated, cultured, and identified according to a previously described method with modifications (25, 26). Described briefly, C57BL/6 female mice were sacrificed and cesarean sections were performed to obtain placentas on day 11 of gestation. Placentas were separated from the underlying endometria using dissecting forceps in a sterile dish containing endothelial cell growth media-2 (EGM-2; Lonza) under a biological dissection microscope. The placentas were cut into small pieces in size of 1–2 mm^2, washed once with EGM-2, and then incubated in dissociation medium (wash medium containing 1 mg/ml collagenase [Sigma-Aldrich, St. Louis, MO], 20 μg/ml DNase [Sigma-Aldrich]) for 1 h at 37˚C with periodic pipetting to separate cells. Cells were washed to remove dissociation medium and then collected and filtered to remove undigested tissue. The cells were separated on an isotonic 40% Percoll gradient (Stemcell Technologies). The trophoblast cell layer was collected and plated onto Matrigel-coated flasks and cultured in EGM-2 medium with 10% FBS (FBS; American Type Culture Collection) and penicillin/streptomycin (American Type Culture Collection). Cells were identified as PMTs by labeling the cells with rabbit anti-mouse cytokeratin 7 (Abcam). Three-six passages were used for experimental detection.

Isolation of MAECs from wild type C57BL/6, CAV-1$^{-/-}$, TLR4$^{-/-}$ female mice

MAECs were isolated and cultured as described previously with minor modifications (27). Described briefly, 8–12-week-old C57BL/6, CAV1$^{-/-}$, and TLR4$^{-/-}$ female mice were sacrificed to obtain MAECs. The aortas were dissected and separated from the aortic arches to the abdominal aortas under a biological dissection microscope without stretching, and immersed in EGM-2 (Lonza) containing 1000 U/ml heparin (Sigma-Aldrich), 50 ng/ml endothelial cell growth supplement (BD Biosciences), and penicillin-streptomycin. The periadventitial fat around the vessels was carefully cleaned under a dissection microscope using forceps and iris scissors. After opening the vessels longitudinally and washing once with EGM-2, three mice aortas were cut into small pieces of 1–2 mm^2, placed in a Matrigel-coated six-well culture plate with 0.5 ml medium, and incubated at 37˚C in a 5% CO_2 incubator; 1.5 ml of medium was carefully added after the explants were incubated for 6 h. The explants were removed and discarded after 5–7 d in culture, and 0.25% trypsin was used to detach cells for further subculture. The cells were identified as endothelial cells by labeling the cells with von Willebrand factor-VII (VWF-VII; Abcam), and uptake of 1,1′-dioctadecyl-1,3,3,3′,3′-tetramethyl-indocarbocyanine-acetylated low-density lipoprotein (DiI-Ac-LDL; Biomedical Technologies, Stoughton, MA). Tube formation was used to assess the specific endothelial cell characteristics. Two-five passages were used for experimental detection.

Culture of JEG-3 cell line

The JEG-3 cell line (American Type Culture Collection) was cultured in EGM-2 medium supplemented with 5% FBS (American Type Culture Collection) at 37˚C in a 5% CO_2 incubator.

HMGB1 gene silencing of PMTs and JEG-3 cell line by small interfering RNA

Transfection of the JEG-3 cell line and PMTs by small interfering RNA (siRNA) was conducted as previously described, with minor modifications (28). PMTs and the JEG-3 cell line (2×10^5 cells/well) were plated into a six-well culture plate (Thermo Fisher Scientific, Roskilde, Denmark). JEG-3 cells at 60–70% confluence were transfected with 5 μl Lipofectamine 2000 (Invitrogen, Carlsbad, CA) and HMGB1-siRNA or scramble-siRNA (Santa Cruz, CA; at a final concentration of 2 μM) in the absence of antibiotics for a period of 24 h. After treatment with siRNA-HMGB1 for 24 h, the CM was replaced with EGM-2 medium supplemented with 5% FBS. Specific silencing was confirmed by Western blot and cell viability was detected with 3-(4,5-dimethylthiazol-2-yl)-2,5-diphenyltetrazolium bromide (MTT; Invitrogen) assay. Experiments were performed on six separate occasions.

Hypoxia of PMTs and JEG-3 cells

Hypoxic conditions were created by placing the cells into a modular incubator chamber (Billups-Rothenburg, Del Mar, CA) flushed with a hypoxic gas mixture containing 1% O_2, 5% CO_2, and 94% N_2 (we selected 1% O_2, as it was shown to elicit a hypoxic response in pilot studies). The oxygen level in the uterus at the time of implantation is 15–18.9 mm Hg in normal pregnancy (29, 30) and the increased number of syncytial knots in the placenta from pregnancies complicated by PE can be replicated in vitro by 1% hypoxia, supporting the idea of 1% hypoxia involvement in the pathogenesis of PE and use in an in vitro trophoblast hypoxia model) (31). PMTs and JEG-3 cells incubated under normoxic conditions (21% O_2) served as controls (JEG3 and PMTs have adapted). The CMs of PMTs and JEG-3 cells were then collected after centrifugation to remove immunoprecipitates and were stored at −80˚C for detection of HMGB1 or culturing of MAECs or HUVECs (32). PMTs and JEG-3 cells were collected to detect HMGB1 protein expression.

Culture of HUVEC cell line

Pooled HUVECs (Lonza) were maintained with EGM-2 (Lonza) in a 37˚C incubator with 5% CO_2. Experiments were performed with cells (passage 3-8) seeded in six-well plates at a density of 2×10^5 cells/well in EGM-2 without supplementation of antibiotics.

TLR4 and CAV-1 gene silencing of HUVECs by siRNA

Inhibition of TLR4/CAV-1 mRNA translation was performed using siRNA targeted to TLR4 mRNA or CAV-1 mRNA (Santa CruzBiotechnology) as described previously with minor modifications (33, 34). Described briefly, 2×10^5 HUVECs were seeded in six-well plates. HUVECs at 60–70% confluence were transfected with Lipofectamine 2000 (Invitrogen) and TLR4-siRNA (at a final concentration of 10 pmol)/CAV-1 siRNA (at a final concentration of 10 nmol) or scramble-siRNA (Santa Cruz, CA) in the absence of antibiotics for a period of 24 h. Following washing in PBS, the cells were replaced with JEG-3 CM for an additional 24 h. Total protein was collected for analysis. Specific silencing was confirmed by Western blot. Cell viability was tested via MTT (Invitrogen, Carlsbad, CA) assay. Experiments were performed on six separate occasions.

MAECs and HUVECs treated with PMTs/JEG-3 CM

MAECs (passage 2-5) and HUVECs (passage 3-8) were seeded in six-well plates at a density of 2×10^5 cells/well in EGM-2 without supplementation of antibiotics. Cells at 60–70% confluence were added to PMTs/JEG-3 CM and incubated at 37°C for 24 h (32). MAECs and HUVECs were collected and stored at −80°C for protein extraction and Western blot.

MAECs and HUVECs treated with HMGB1

MAECs (passage 2-5) and HUVECs (passage 3-8) were seeded in six-well plates at a density of 2×10^5 cells/well in EGM-2 without supplementation of antibiotics. Cells at 60–70% confluence were added to recombinant HMGB1 (rHMGB1) at a final concentration of 1 μg/ml and incubated at 37°C for 24 h (6). MAECs and HUVECs were collected and stored at −80°C for protein extraction and Western blot.

MTT assay to assess cell viability

Cells were seeded in a 96-well microplate at 4000 cells in 100 μL per well. Each group had five duplicate wells. To measure cell proliferation, the CM in each 96-well plate was changed to serum-free conditions after 24 h of seeding, and MTT (Invitrogen) assay was performed after different conditional treatments. MTT assay was performed at the end of each treatment following routine procedure (35). The experiment was repeated six times to ensure data reproducibility.

Evaluation of JEG-3 cells and PMTs mitochondrial potential by JC1

5,5′,6,6′-Tetrachloro-1,1′,3,3′-tetraethylbenzimidazolylcarbocyanine iodide (JC1; Invitrogen) is a cationic dye that exhibits potential-dependent accumulation in the mitochondria, indicated by a fluorescence emission shift from green (~525 nm) to red (~590 nm). JC1 monomers were detected with a green filter. JC1 dimers that formed on mitochondrial membranes with high mitochondrial potential were detected via a red filter. Consequently, mitochondrial depolarization was indicated by a decrease in the red/green fluorescence intensity ratio (36). We plated 50,000 JEG-3 cells and PMTs in six-well plates. JEG-3 cells and PMTs were cultured in 1% oxygen and 21% oxygen (control) for 24 h. JEG-3 cells and PMTs were stained for 10 min in medium containing JC1 (at a final concentration of 50 μg/ml) and Hoechst 33325 (Sigma-Aldrich; at a final concentration of 1 μg/ml). JEG-3 cells and PMTs were washed three times with PBS (Sigma-Aldrich). Pictures were taken using a Nikon TE 200 inverted epifluorescence microscope (Melville, NY) equipped with a digital camera (CoolSNAP HQ2; Photometrics, Tucson, AZ) and micrographs were processed with AxioVision 4.8 software (Carl Zeiss).

Analysis of JEG-3 cells and PMTs apoptosis

JEG-3 cells and PMTs apoptosis were detected by Alexa Flour 488 Annexin V/Dead Cell Apoptosis Kit (Invitrogen) to detect early apoptotic cells (cells with intact membranes with externalized phosphatidylserine residues), late apoptotic cells (apoptotic cells showing compromised membrane integrity), and nonapoptotic cells at 24 h of culture (37). Cells were washed in ice-cold PBS (Sigma-Aldrich) and resuspended in 100 ml annexin V binding buffer (140 mmol/L NaCl, 2.5 mmol/L $CaCl_2$, 1.5 mmol/L $MgCl_2$, and 10 mmol/L HEPES, pH 7.4) containing annexin V-FITC and propidium iodide (PI; 1 μg/ml) for 15 min. Cells were analyzed by FACS using Guava Express Pro 8.1 software.

Immunofluorescence analysis

Immunofluorescence analysis was performed as previously described (38). JEG-3 cells and PMTs were cultured in 1% oxygen or 21% oxygen for 24 h. The cells were washed with PBS (Sigma-Aldrich) and fixed in 4% paraformaldehyde. The cells were incubated first with rabbit anti-HMGB1 (Abcam), and mouse anti-Actin Ab (Abcam) and then reacted with their corresponding PE-conjugated monkey anti-rabbit IgG (BD Biosciences) and FITC-conjugated goat anti-mouse IgG (BD Biosciences) as secondary Abs. To visualize the nuclei, the cells were stained with DAPI (blue; Sigma-Aldrich). Fluorescent images were observed under a laser-scanning confocal microscope (Bio-Rad, MRC-1024ES), and micrographs were processed with AxioVision 4.8 software (Carl Zeiss).

Real-time PCR

JEG-3 cells and PMTs were cultured in 1% oxygen or 21% oxygen for 24 h. After harvesting, JEG-3 cells and PMTs were immediately submerged in RNAlater RNA stabilization reagent (Ambion, Austin, TX), according to the manufacturer's instructions, processed for RNA isolation, and stored at −80°C for further analysis. RNA expression of HMGB1 (upper TC AAAGGAGAACATCCTGGCCTGT, lower CTGCTTGTCATCTGCAG-CAGTGTT) and 18S rRNA (upper 5′-CGG GTC GGG AGT GGG T-3′, lower 5′-GAA ACG GCT ACC ACA TCC AAG-3′) (Qiagen, Valencia, CA) was quantified with a SYBR Green two-step real-time RT-PCR Kit (Qiagen, Valencia, CA) as described previously (39). 18S rRNA was used as an endogenous control. Each sample was estimated in triplicate on the CFX manager 2.1 program (Bio-Rad). Real-time PCR data were plotted as the Δ Rn fluorescence signal versus the cycle number. An arbitrary threshold was set to the midlinear portion of the log Δ Rn cycle plot. The threshold cycle was defined as the cycle number at which the Δ Rn crossed this threshold. The best combination of reference genes was automatically calculated by the CFX manager 2.1 program (Bio-Rad) based on M-value.

Western blot

Western blot was performed as described previously (40). Proteins were extracted from cultured cells using CelLytic MT Cell Lysis Reagent (Sigma-Aldrich) and separated on SDS-polyacrylamide gels. Proteins were probed with the following Abs: rabbit anti-HMGB1 (1:1000; Abcam), rabbit anti-TLR4, rabbit anti-TLR2, rabbit anti-RAGE, rabbit anti-VE-cadherin, rabbit anti-caveolin (1:200; Santa Cruz Biotechnology); mouse anti-actin (1:1,000, Santa Cruze) was used as an internal control. Secondary Abs used were IR Dye 700–conjugated anti-rabbit (1:4000) and IR Dye 800-conjugated anti-mouse (1:5000; BD Biosciences). The blots were scanned with an Odyssey imager (LI-COR Biosciences) and band intensity was determined with Quantity One System (Bio-Rad).

In vitro permeability assay of HUVECs or MAECs

Permeability was quantified by spectrophotometric measurement of the flux of Evans blue-bound albumin across functional HUVEC monolayers using a modified two-compartment chamber model as previously described (41). Described briefly, HUVECs or MAECs were plated (5×10^4 cells/well) in 4-μm pore size and 12-mm diameter transwells for 3 d. The confluent monolayers were incubated with trophoblasts (JEG-3 cells and PMTs) CM or rHMGB1 (1 μg/ml) for 24 h. Inserts were washed with PBS (Sigma-Aldrich), pH 7.4, before addition of 0.5 ml of 0.67 mg/ml Evans blue (Sigma-Aldrich) diluted in growth medium containing 4% BSA (Sigma-Aldrich). Fresh growth medium was added to the lower chamber, and the medium in the upper chamber was replaced with Evans blue/BSA. After 10 min, the OD at 650 nm was measured in the lower chamber. Experiments were performed in triplicate and repeated six times.

FITC-BSA HUVEC staining

To visualize whether 24-h hypoxic JEG-3 cells/PMTs CM regulates the FITC-BSA uptake in HUVECs/MAECs, 50,000 HUVECs/MAECs were seeded in a six-well plate and incubated for 24 h to achieve 75% confluence. The HUVECs/MAECs were treated with JEG-3 cells/PMTs CM for an additional 24 h. FITC-BSA uptake of HUVEC/MAECs was performed as previously described with minor modifications (42). FITC-BSA (Sigma-Aldrich; at a final concentration of 0.5 mg/ml) and Hoechst 33325 (Sigma-Aldrich; at a final concentration of 1 μg/ml) were added to the cells and incubated for 30 min. The cells were washed three times with PBS. Pictures were taken using a Nikon TE 200 inverted epifluorescence microscope equipped with a digital camera (CoolSNAP HQ2), and micrographs were processed with AxioVision 4.8 software (Carl Zeiss).

ELISA

The cell culture medium from PMT and JEG-3 cells under various conditions was collected and used to determine HMGB1 levels with an ELISA kit (IBL, Gunma, Japan) according to the manufacturer's instructions.

Immunoprecipitation assay

Immunoprecipitation assay was performed as described previously (43). HUVEC lysates or kidney lysates of C57BL/6 mice containing 200 μg of total protein were incubated with rabbit anti-CAV-1 (Abcam; 1/100 v/w) or rabbit IgG (Santa Cruz Biotechnology) for 2 h at 4°C on a rotating device, followed by the addition of Protein A-G PLUS Agarose (Santa Cruz Biotechnology) overnight under the same conditions. Immunoprecipitation complexes were washed three times with 500 μl lysis buffer containing protease inhibitor (Sigma-Aldrich; pH = 7.5). Supernatants were discarded, and pellets were resuspended in 20 μl lysis sample buffer. After 7 min of boiling, samples were centrifuged and analyzed by Western blotting with Ab against TLR4. For TLR4 immunoprecipitation, goat anti-TLR4 (1/100 v/w) or goat IgG (Santa Cruz Biotechnology) were used to pull down protein before Western blotting with Ab against CAV-1.

Statistical analyses

Values are reported as mean ± SD. All statistical analyses were two-sided and were performed with SPSS statistical software version 15.0 (SPSS, Chicago, IL). For all experiments, the Kruskal–Wallis test was used to determine differences among the groups. When a significant difference between groups was found, multiple comparisons were performed using the Bonferroni procedure with type-I error adjustment. A p value < 0.05 was considered statistically significant.

Results

Identifications of MAECs and PMTs

MAECs were identified as endothelial cells by labeling the cells with rat anti-mouse vWF and confirming the uptake of DiI-Ac-LDL and tube formation (Fig. 1B, 1D, 1F). HUVECs were detected as control (Fig. 1A, 1C, 1E). PMTs were identified as trophoblast cells by labeling the cells with rabbit anti-mouse cytokeratin 7 (Abcam; Fig. 1G, 1I). JEG-3 cells were stained as control (Fig. 1H, 1J).

Hypoxic trophoblasts (both JEG-3 cells and PMTs) displayed higher HMGB1 mRNA, intracellular HMGB1 protein, and HMGB1 in CM than those of normoxic trophoblasts

To detect whether hypoxia increases trophoblast (including JEG-3 cells and PMTs) HMGB1 protein expression and CM HMGB1 level, JEG-3 and PMT cells were cultured in 1% oxygen for 0, 2, 4, 8, 24, and 48 h. The HMGB1 level in supernatants and the HMGB1 cell protein was increased in trophoblasts (including JEG-3 cells and PMTs) cultured in hypoxic conditions (1% oxygen) for 24 and 48 h compared with those cultured in normoxic conditions (21% oxygen; $n = 6$; Fig. 2A–F).

To detect the HMGB1 mRNA expression of hypoxic trophoblasts (JEG-3 cells and PMTs), JEG-3 cells and PMTs were cultured in 1% oxygen or 21% oxygen for 24 h. Real-time RT-PCR was used to detect HMGB1 mRNA expression. HMGB1 mRNA levels were increased in trophoblasts (JEG-3 cells and PMTs) cultured in hypoxic conditions (1% oxygen) for 24 h as compared with those cultured under normoxic conditions (21% oxygen; $n = 6$; Fig. 2G). We also detected the HMGB1 protein expression of trophoblasts (JEG-3 cells and PMTs) by using immunofluorescence analysis. The HMGB1 protein expression of hypoxic trophoblasts (JEG-3 cells and PMTs) was significantly higher than those of normoxic trophoblasts (JEG-3 cells and PMTs; $n = 6$; Fig. 3).

Hypoxia decreased trophoblasts (JEG-3 cells and PMTs) viability and increased trophoblasts (JEG-3 cells and PMTs) apoptosis

Cell (JEG-3 cells and PMT) viability of hypoxic trophoblasts was decreased after 24 and 48 h of culture in hypoxic conditions (1% oxygen) compared with those cultured under normoxic conditions (21% oxygen; $n = 6$; Fig. 4A, 4B). Apoptosis in trophoblasts (JEG-3 cells and PMTs) was assessed with FITC-annexin V and PI staining (BD Biosciences) and flow cytometric analysis (BD FACSCalibur). The apoptosis of hypoxic trophoblasts (JEG-3 cells and PMTs) was significantly higher than that of normoxic trophoblasts (JEG-3 cells and PMTs; $n = 6$; Fig. 4C–G).

Twenty-four hours of hypoxia decreased trophoblasts (JEG-3 cells and PMTs) mitochondrial membrane potential

To detect the mitochondrial membrane potential and apoptosis of hypoxic trophoblasts (JEG-3 cells and PMTs), trophoblasts (JEG-3 cells and PMTs) were cultured in 1% oxygen and 21% oxygen for 24 h. The mitochondrial membrane potential was detected by JC1 staining assay. Trophoblasts (JEG-3 cells and PMTs) were also stained with Hoechst 33325.Twenty-four hours of hypoxia decreased the trophoblasts' (JEG-3 cells and PMTs) mitochondrial membrane potential as compared with normoxia (21% oxygen; $n = 6$; Fig. 5).

Silencing HMGB1 in JEG-3 cells and PMTs

HMGB1 siRNA silenced 81.89% of JEG-3 HMGB1 protein expression and 82.5% of PMT HMGB1 protein expression, but did not affect the viability of JEG-3 cells and PMTs at the final concentration of 2 μmol (Fig. 6A–C; $n = 6$). In addition, HMGB1 siRNA silenced 80.7% of hypoxia JEG-3 HMGB1 protein expression and 83.4% of hypoxia PMT HMGB1 protein expression, and it decreased 88% of hypoxia JEG-3-CM HMGB1 level and 89.2% of hypoxia PMTs-CM HMGB1 level at the final concentration of 2 μmol (Fig. 6D–F; $n = 6$). Therefore, we used the concentration of 2 μmol for the following experiment.

HMGB1 from hypoxic trophoblasts (JEG-3 cells and PMTs) increased the permeability of the endothelial cell (HUVEC and MAEC) monolayer

First, to detect whether HMGB1 released by hypoxic trophoblasts (JEG-3 cells and PMTs) increases endothelial cell permeability, HUVECs were treated with the 24-h normoxic CM and hypoxic trophoblasts (JEG-3 cells and PMT) for 0, 4, 8, 12, 24, and 48 h, respectively. HUVEC permeability was detected by Evans blue

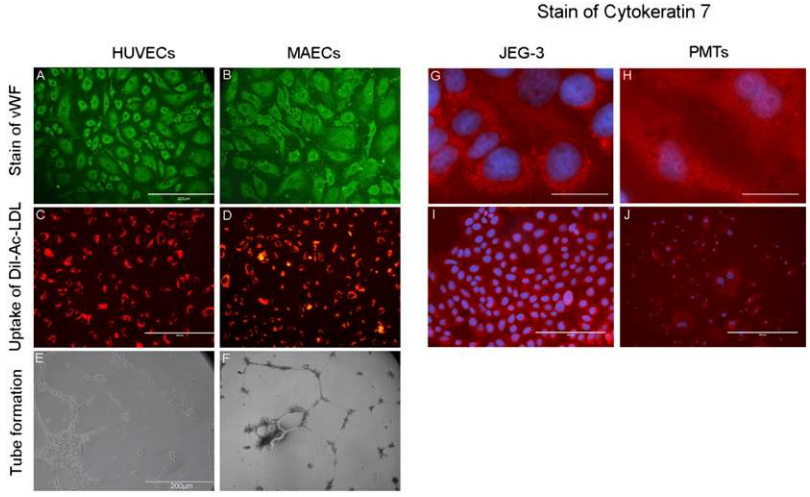

FIGURE 1. Characterization of C57BL/6 MAECs and PMTs. Subconfluent HUVECs (**A**) and MAECs (**B**) (second passage) grown on glass cover slips were stained with an endothelial surface marker, vWF, using anti-vWF Ab (primary) and a FITC-labeled secondary Ab. Uptake of DiI-Ac-LDL in subconfluent HUVECs (**C**) and MAECs (**D**) grown on glass cover slips. Tube formation of subconfluent HUVECs (**E**) and MAECs (**F**) grown on growth factor–reduced Matrigel plate. Images were taken after 4 h of incubation. Scale bar, 200 μm. Characterization of PMTs from C57BL/6 pregnant mice. Subconfluent JEG-3 cells (**G** and **I**) and PMTs (**H** and **J**) grown on glass coverslips were stained with a trophoblast marker, cytokeratin 7, by using anti-cytokeratin 7 Ab (primary) and a PE-labeled secondary Ab. Scale bar, 100 μm (I and J). Scale bar, 200 μm (G and H).

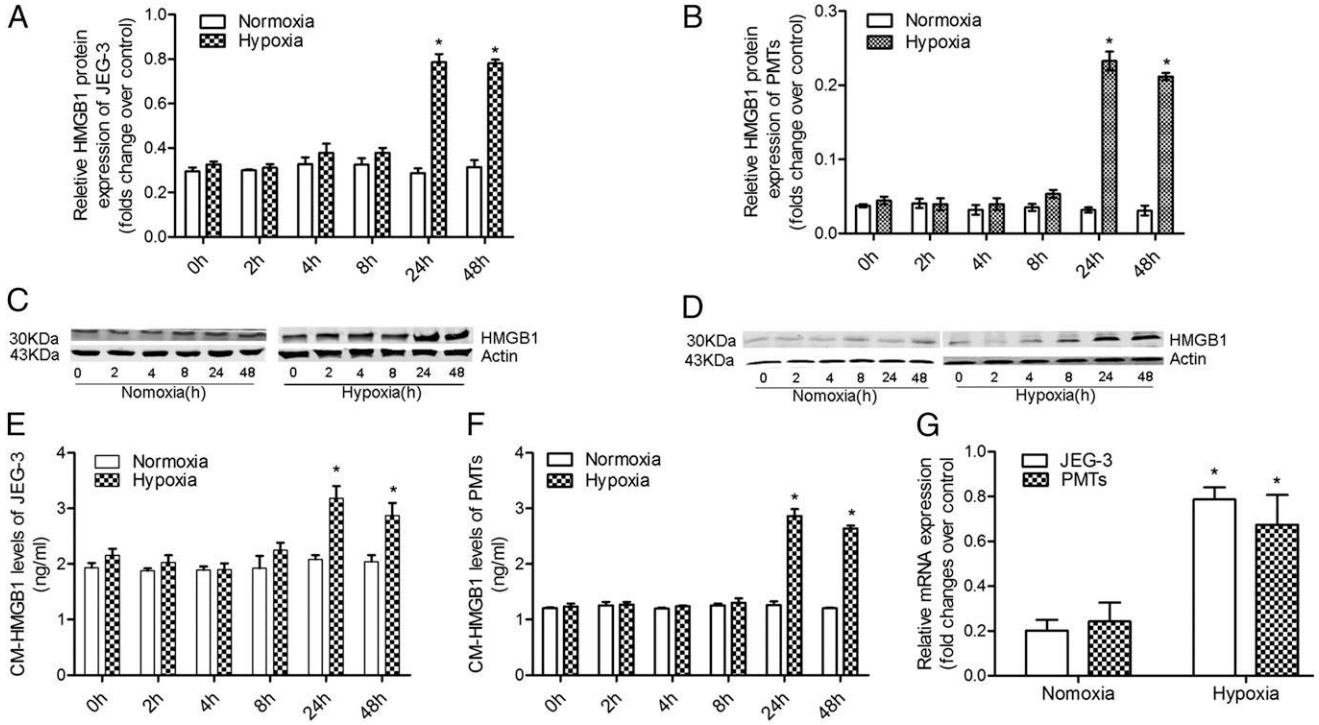

FIGURE 2. HMGB1 levels of CM, HMGB1 protein expression, and mRNA expression in JEG-3 cells and PMTs at different time points under hypoxic conditions. (**A** and **B**) Bar graph illustrating the protein expression of HMGB1 at different hypoxic JEG-3 cells (A) and PMTs (B) time points. (**C** and **D**) Representative photographs of Western blot of HMGB1 protein expression at different time points of hypoxia JEG-3 cells (C) and PMTs (D). (**E** and **F**) Bar graph illustrating CM HMGB1 levels at different hypoxic time points of JEG-3 cells (E) and PMTs (F). CM HMGB1 levels of JEG-3 cells and PMTs were detected by ELISA kit of HMGB1. Values were reported as mean ± SD ($n = 6$). (**G**) HMGB1 mRNA induction in hypoxic JEG-3 cells and PMTs. The bar graph shows the quantitative RNA measurement using Bio-Rad CFX manager 2.1 (admin). Values were reported as mean ± SD ($n = 6$). $^{*}p < 0.05$, compared with normoxia.

labeled-BSA. We found that the 24-h hypoxic trophoblast CM (JEG-3 cells and PTM) significantly enhanced the permeability of HUVECs incubated for 24–48 h compared with 24-h normoxic trophoblast CM (JEG-3 cells and PMT; 21% oxygen; $n = 6$; Fig. 7A, 7B).

Second, to test whether the hypoxic trophoblast CM increased endothelial cell permeability via HMGB1, we used 2 μmol/L HMGB1 siRNA to silence the HMGB1 protein expression of JEG-3 cells and PMT before hypoxia, and we detected the effect of the hypoxic trophoblast CM on the endothelial cell (HUVEC and MAEC) monolayer permeability. We also applied 1 μg/ml rHMGB1 to deal with the endothelial cell monolayer for 24 h to determine whether rHMGB1 increases endothelial cell (HUVEC and MAEC) monolayer permeability. Our data show that the increased endothelial cell permeability (HUVECs and MAECs) by 24-h hypoxic trophoblast (JEG-3 cell and PMTs) CM was re-

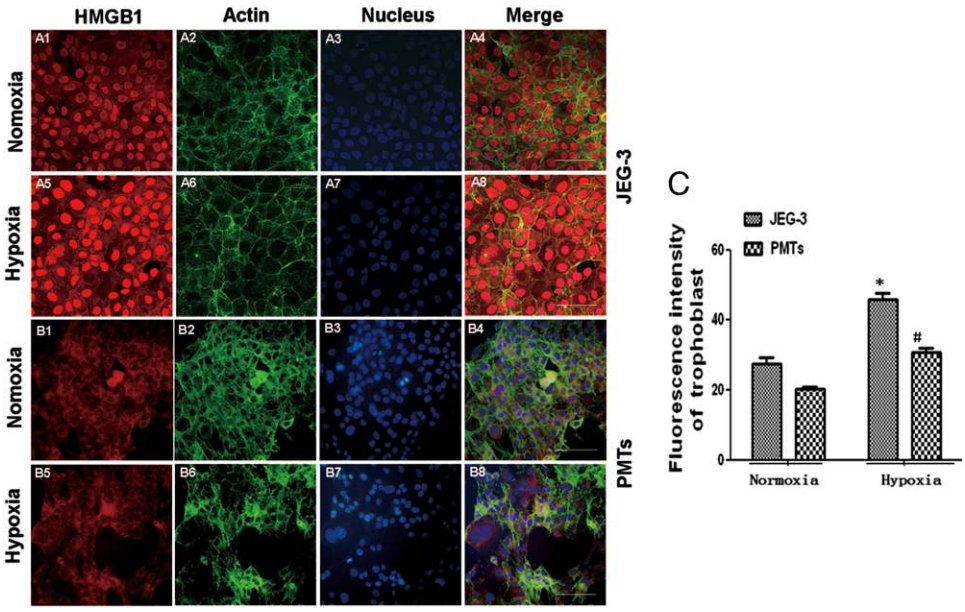

FIGURE 3. (**A** and **B**) The HMGB1 protein expression of hypoxic and normoxic JEG-3 cells (A_1–A_8) and PMTs (B_1–B_8) was detected by immunofluorescence analysis. (**C**) Bar graph illustrating the red fluorescence intensity (HMGB1) of JEG-3 cells and PMTs. The red fluorescence intensity (HMGB1) of hypoxic JEG-3 cells and PMTs were significantly higher than that of the normoxic JEG-3 cells and PMTs. Values were reported as mean ± SD ($n = 6$). Scale bar, 100 μm. $^{*}p < 0.05$, $^{\#}p < 0.05$, compared with normoxia.

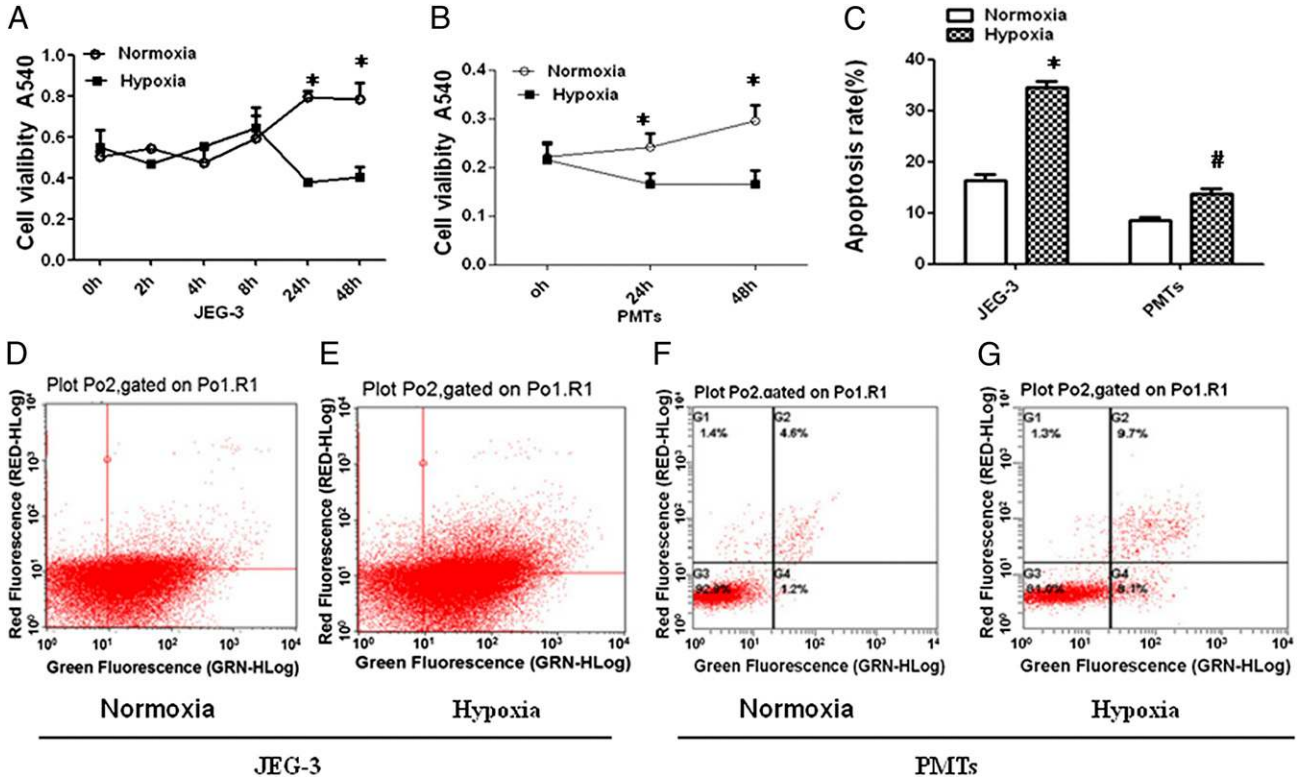

FIGURE 4. Trophoblast (JEG-3 cells and PMTs) viability and trophoblast (JEG-3 cells and PMTs) apoptosis of hypoxic trophoblasts was detected by MTT and annexin V/PI staining. (**A** and **B**) Cell viability of the JEG-3 cells (A) and PMTs (B) decreased significantly after 24 h of incubation with 1% oxygen as compared with 21% oxygen. Values were reported as mean ± SD ($n = 6$). $^{*}p < 0.05$, $^{\#}p < 0.05$, compared with normoxia. (**C**–**G**) Hypoxia induces apoptosis in hypoxic trophoblast (JEG-3 cells and PMTs). (C) Quantitative analysis of apoptotic cells in normoxic and hypoxic trophoblast (JEG-3 cells and PMTs). Values were reported as mean ± SD ($n = 6$). $^{*}p < 0.05$, compared with normoxia. (D–G) Representative annexin-V/PI staining assay of normoxic (D and F) and hypoxic trophoblast (JEG-3 cells and PMTs) (E and G).

versed by HMGB1 (JEG-3 and MPT) silencing before hypoxia in trophoblasts. HMGB1 (1 μg/ml) also significantly enhanced the permeability of endothelial cells (HUVECs and MAECs) after 24 h of incubation as compared with the control ($n = 6$; Fig. 7C, 7D).

Silencing TLR4 and CAV-1 in HUVECs

Transfection with 10 pmol TLR4-siRNA significantly decreased TLR4 protein expression in HUVECs by 82.4% without affecting viability and expressions of TLR2 and TLR9 protein expression in

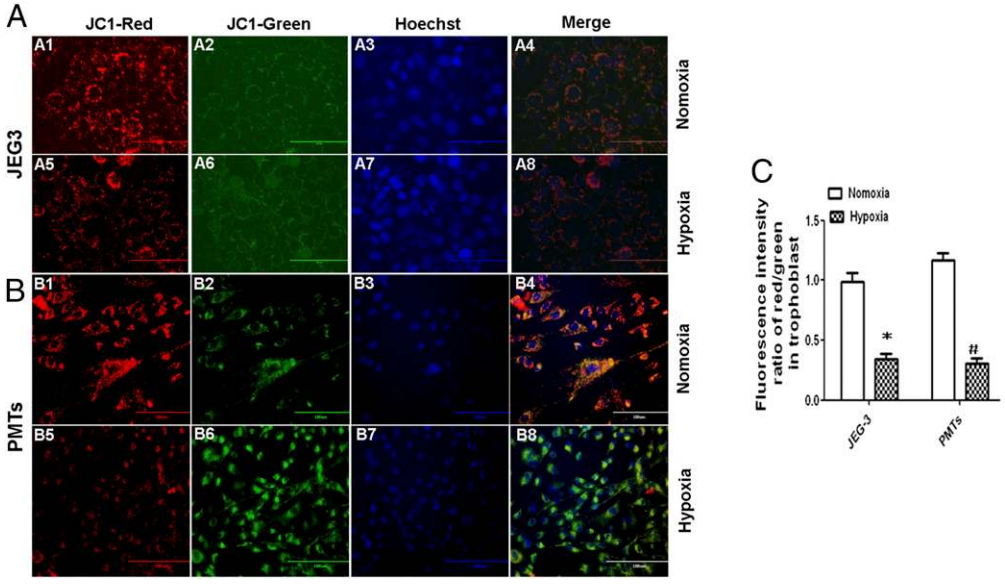

FIGURE 5. Effect of hypoxia on trophoblast (JEG-3 cells and PMTs) mitochondrial membrane potential. Micrographs illustrate JC-1 accumulation in (**A**) the mitochondria of normoxic and hypoxic JEG-3 cells and (**B**) PMTs. Scale bar, 100μm. (**C**) The red/green fluorescence intensity ratio of hypoxic trophoblast (JEG-3 cells and PMTs) was significantly lower than that of the normoxic trophoblast (JEG-3 cells and PMTs). Values were reported as mean ± SD ($n = 6$). $^{*}p < 0.05$, $^{\#}p < 0.05$, compared with normoxia.

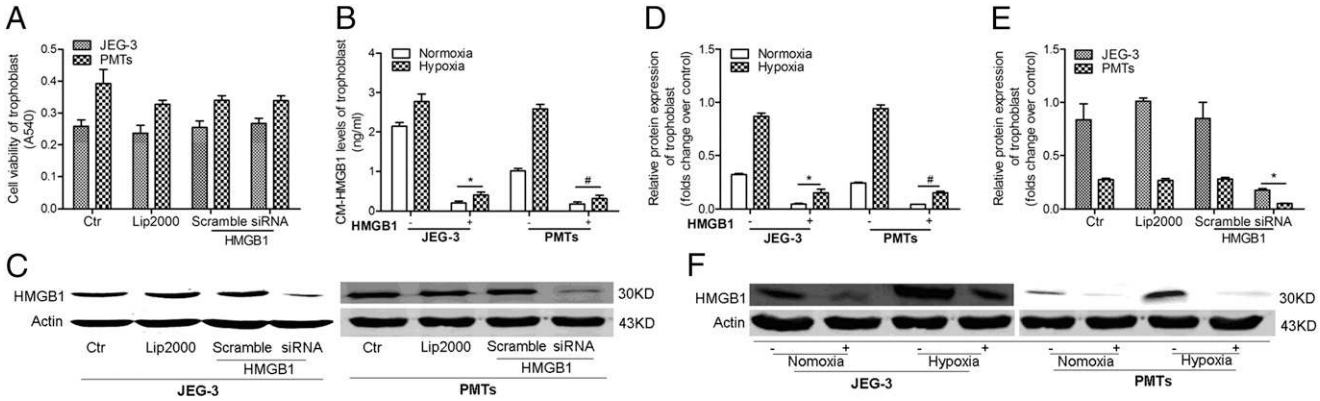

FIGURE 6. HMGB1 silencing of JEG-3 cells and PMTs. (**A**) The cell viability of JEG-3 cell lines and PMTs was not affected by transfection of 2 μmol HMGB1 siRNA. (**B**) HMGB1 siRNA silenced ~81.89% of JEG-3 HMGB1 protein expression and 85.29% of PMT HMGB1 protein expression. Values were reported as mean ± SD ($n = 6$). $^{*}p < 0.05$, compared with Ctr. (**D** and **E**) HMGB1 siRNA also silenced 80.7% of hypoxia JEG-3 HMGB1 protein expression and 83.4% of hypoxia PMT HMGB1 protein expression (D), and decreased 88% of hypoxia JEG-3-CM HMGB1 level and 89.2% of hypoxia PMTs-CM HMGB1 level (E) at the final concentration of 2 μmol. Values are reported as mean ± SD ($n = 6$). $^{*}p < 0.05$, $^{\#}p < 0.05$, compared with Ctr. (**C** and **F**) Representative blots of JEG-3 and PMTs HMGB1silencing are shown. Ctr, endothelial cells incubated with EGM-2; Lip2000, Lipofectamine 2000.

HUVECs. CAV-1-siRNA decreased CAV-1 protein expression of HUVECs by 80.2% without affecting the viability of HUVECs at the final concentration of 10 nmol. Therefore, we used 10 pmol as the final transfection concentration of TLR4 and 10 nmol as the final transfection concentration of CAV-1. (Fig. 8).

HMGB1 released from hypoxic trophoblasts (JEG-3 cells and PMTs) enhanced the permeability of endothelial cells (HUVECs and MAECs) via the TLR4-CAV-1 pathway

We assessed whether HMGB1 released from hypoxic trophoblasts increased endothelial cell permeability via the TLR4 (TLR2, RAGE)–CAV-1 pathway.

First, we detected the TLR4, TLR2, RAGE protein expression of HUVECs incubated with different time points of hypoxia JEG-3 CM. Our data showed that 24-h hypoxia JEG-3 CM increased the TLR4 protein expression of HUVECs, but did not increase TLR2 and RAGE protein expression (Fig. 9A, 9C). We also got the same results in MAECs incubated with different time points of hypoxia PMTs-CM (Fig. 9B, 9D). rHMGB1 increased the TLR4 protein expression, but did not increase TLR2 and RAGE protein expression of HUVECs/MAECs (Fig. 9E–H).

Second, we detected the TLR4 and CAV-1 protein expression of HUVECs/MAECs incubated with 24-h hypoxia JEG-3 cells/PMTs CM and rHMGB1. Our data showed that 24-h hypoxia JEG-3 CM and rHMGB1 increased the TLR4 and CAV-1 expression of HUVECs after incubation for 24 h at the same time; 24-h hypoxic PMT CM and rHMGB1 also induced the TLR4 and CAV-1 protein expression of MAECs (Fig. 10A–D).

Third, the HMGB1 silencing of trophoblasts (including JEG-3 and PMT cells) before hypoxia inhibited the hypoxia-induced endothelial cells TLR4 and CAV-1 protein expression, including HUVECs and MAECs (Fig. 10A–D). TLR4 or CAV-1 silencing OF HUVECs (siRNA) and TLR4$^{-/-}$ or CAV-1$^{-/-}$ MAECs (gene knockout) reversed the hypoxic trophoblast-induced permeability of endothelial cells ($n = 6$; Fig. 10E, 10F).

Twenty-four-hour hypoxic JEG-3 cell CM increased the FITC-BSA HUVEC uptake

To test whether 24-h hypoxic trophoblast (JEG-3 cells and PMTs) CM could increase the uptake of BSA in ECs (HUVECs and MAECs), FITC-BSA staining was used to detect the BSA endocytosis of hypoxic trophoblasts (JEG-3 cells and PMTs) CM-

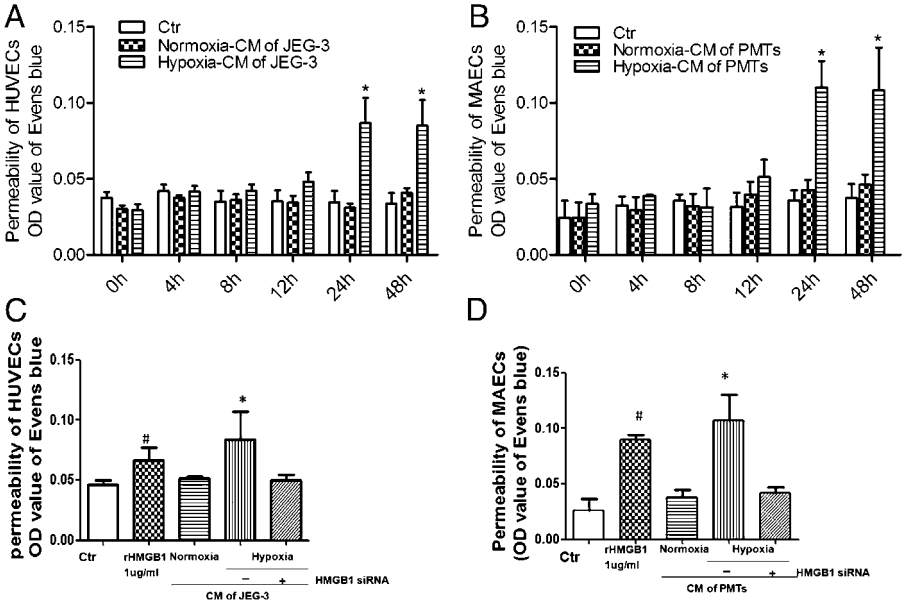

FIGURE 7. Permeability response to CM of trophoblast and rHMGB1. Endothelial permeability was assessed by Evans blue labeled-BSA. (**A** and **B**) Endothelial cells (HUVECs and MAECs) incubated in 24 h normoxic CM, 24-h hypoxic trophoblast (JEG-3 cells and PMTs) CM for 0, 2, 4, 8, 24, and 48 h. Values were reported as mean ± SD ($n = 6$). $^{*}p < 0.05$, compared with 24 h normoxic CM. (**C** and **D**) Endothelial cell monolayers were treated with the 24 h normoxic CM, 24 h hypoxic JEG-3 cells and PMT CM, 24-h hypoxic HMGB1 siRNA transfected-JEG-3 cells CM, and EGM-2 medium with rHMGB1 1 μg/ml incubated for 24 h, respectively. Values were reported as mean ± SD ($n = 6$). $^{*}p < 0.05$ versus normoxia and control, $^{\#}p < 0.05$ versus normoxia and control. Ctr, endothelial cells incubated with EGM-2.

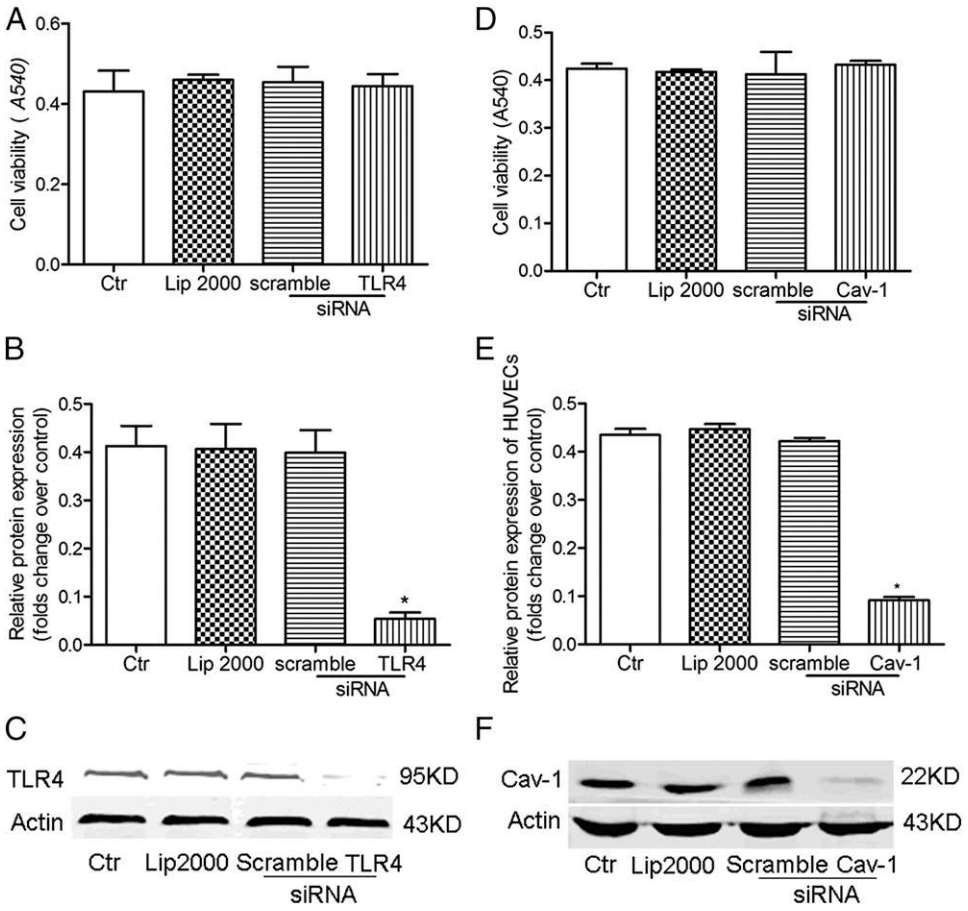

FIGURE 8. TLR4 and CAV-1 silencing by siRNA in HUVECs. (**A** and **B**). The cell viability of HUVECs (A) was not affected by transfection of 10 pmol TLR4 siRNA and silenced 82.4% of the HUVEC TLR4 protein expression (B). (**D** and **E**) CAV-1 siRNA silenced 80.2% of the HUVEC CAV-1 protein expression (E) and did not affect the viability of HUVECs (D) at the final concentration of 10nmol. (**C** and **F**) Representative blots of HUVEC TLR4 (C) and CAV-1 silencing (F) are shown. Values were reported as mean ± SD (n = 6). *p < 0.05, compared with Ctr. Ctr, endothelial cells incubated with EGM-2.

treated ECs (HUVECs and MAECs). The intensity of the cell membranes and BSA endocytosis of hypoxic CM-treated ECs (HUVECs and MAECs) was higher than those of the normoxic trophoblasts CM-treated ECs (HUVECs and MAECs). The HMGB1 silencing of JEG-3 cells before hypoxia and TLR4 or CAV-1 silencing of HUVECs inhibited the hypoxic JEG-3 CM-induced uptake of FITC-BSA (Fig. 11A–H, 11M). In addition, the HMGB1 silencing of PMTs before hypoxia and TLR4$^{-/-}$ or CAV-1$^{-/-}$. MAECs inhibited the hypoxic PMTs CM-induced uptake of FITC-BSA (n = 6; Fig. 11G–L, 11N).

CAV-1 and TLR4 are colocalized in HUVECs and C57BL/6 mouse kidney; CAV-1 is downstream of the HMGB1-TLR4 pathway in the hypoxic trophoblast CM-induced permeability of the endothelial cell monolayer

To detect whether CAV-1 and TLR4 are colocalized in HUVECs and C57BL/6 mouse kidney, we used the coimmunoprecipitation

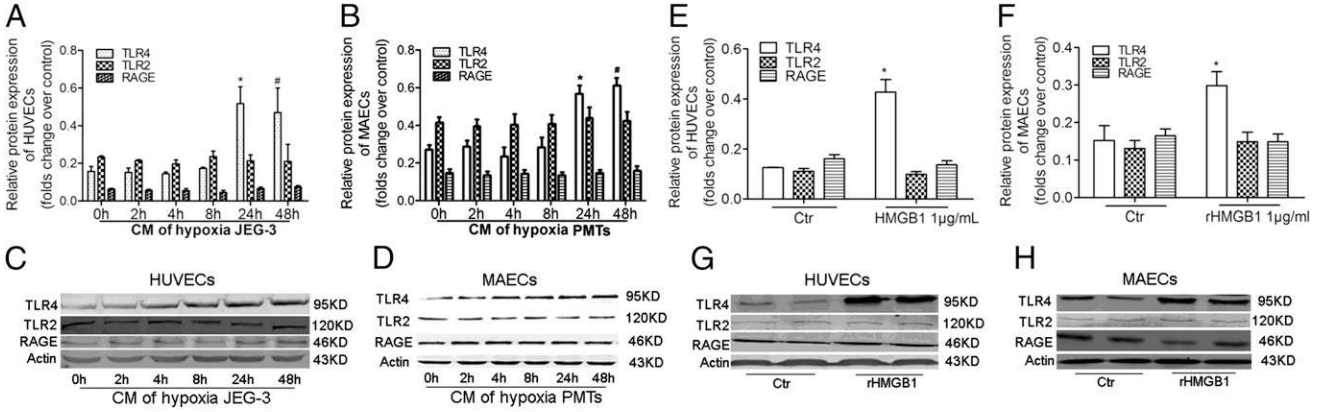

FIGURE 9. TLR4, TLR2, and RAGE protein expression of (**A**) HUVECs and (**B**) MAECs incubated with different time points of trophoblast (JEG-3 cells and PMTs) CM and rHMGB1for 24 h. (A and B) The TLR4, TLR2, and RAGE protein expression in HUVECs and MAECs incubated with different time points of hypoxic trophoblast (JEG-3 cells and PMTs) CM for 24 h. (**C** and **D**) Representative Western blot showing TLR4, TLR2, and RAGE protein expression in HUVECs and MAECs incubated with different time points of hypoxic trophoblast (JEG-3 cells and PMTs) CM for 24 h (n = 6). (**E** and **F**) The TLR4, TLR2, and RAGE protein expression in HUVECs and MAECs incubated with 1 μg/ml rHMGB1 for 24 h (n = 6). (**G** and **H**) Representative Western blot showing TLR4, TLR2, and RAGE protein expression in HUVECs and MAECs incubated with 1 μg/ml rHMGB1 for 24 h.

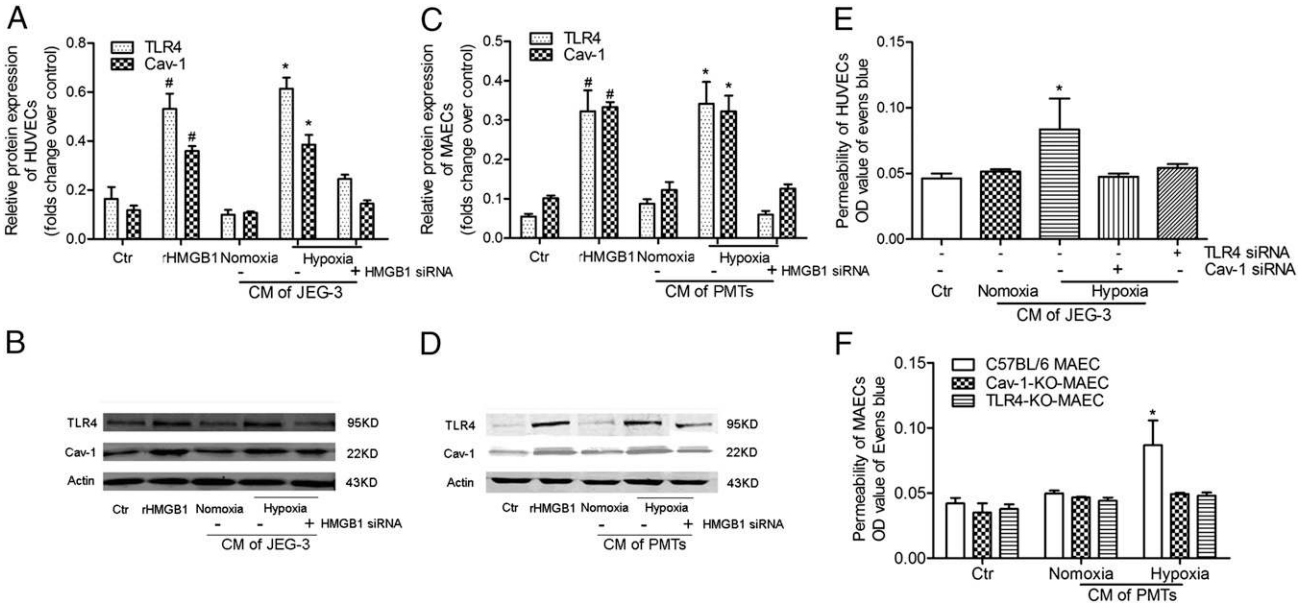

FIGURE 10. Hypoxic trophoblasts (JEG-3 cells and PMTs) enhance the permeability of endothelial cells (HUVECs and MAECs) via the HMGB1-TLR4-CAV-1 pathway. (**A** and **C**) The TLR4 and CAV-1 protein expression in HUVECs and MAECs incubated with 24-h normoxic JEG-3 cells/PMTs CM, hypoxic JEG-3 cells/PMTs CM, hypoxic HMGB1 siRNA-transfected JEG-3 cells/PMTs CM, and EGM-2 medium with rHMGB1 1 μg/ml incubated for 24 h. Values were reported as mean ± SD (n = 6). Ctr, endothelial cells incubated with EGM-2. (**B** and **D**) Representative Western blot photographs of TLR4 and CAV-1 protein expression in HUVECs and MAECs incubated with 24-h normoxic JEG-3 cells/PMTs CM, hypoxic JEG-3 cells/PMTs CM, hypoxic HMGB1 siRNA-transfected JEG-3 cells/PMTs CM, and EGM-2 medium with rHMGB1 1 μg/ml incubated for 24 h. (**E**) The permeability of HUVEC monolayers incubated with 24-h hypoxic JEG-3 cells CM for 24 h after was silenced by TLR4 or CAV-1 siRNA. HUVEC permeability was assessed with Evans blue/BSA. Values were reported as mean ± SD (n = 5). Ctr, endothelial cells incubated with EGM-2. (**F**) The permeability of TLR4$^{-/-}$ and CAV-1$^{-/-}$ MAECs treated with 24-h hypoxic PMT CM. MAECs permeability was assessed with Evans blue/BSA. Values were reported as mean ± SD (n = 6). Ctr, MAECs incubated with EGM-2. *$p < 0.05$, compared with normoxia and Ctr.

assay to test the colocalization of CAV-1 and TLR4 in protein of HUVECs and C57BL/6 mouse kidney. Our data showed that CAV-1 and TLR4 are colocalized in HUVECs and C57BL/6 mouse kidney (n = 3; Fig. 12E, 12F).

To detect the relationship between TLR4 and CAV-1, MAECs from TLR4$^{-/-}$ mice or CAV-1$^{-/-}$ mice were treated with the 24-h CM of hypoxic PMTs and EGM-2 medium with rHMGB1 1 μg/ml incubated for 24 h. The protein expression of TLR4 and CAV-1 in MAECs was detected with Western blot. Our data showed that TLR4 knockout inhibited the 24-h hypoxic PMT-CM and rHMGB1-induced CAV-1 protein expression in MAECs (n = 6; Fig. 12A, 12C). However, CAV-1 knockout did not inhibit the 24 h hypoxic PMT-CM and HMGB1-induced TLR4 protein expression in MAECs (n = 6; Fig. 12B, 12D).

Glycyrrhizic acid attenuated the permeability of the endothelial cell (HUVEC and MAEC) monolayer induced by hypoxia trophoblast (including PMT and JEG-3) CM

In order to detect whether hypoxic trophoblast–induced permeability of endothelial cells is dependent on HMGB1 or not, the following experiments were conducted.

First, to detect the noncytotoxic dose of GA (A) on ECs (include HUVECs and MAECs). ECs (include HUVEC and MAEC) were cultured with EGM2 medium and GA (TCI Development, Shanghai, China) at concentrations ranging from 50 to 500 μg/ml for 24 h. The cells viability were detected with the MTT method. Our data showed that endothelial cell viability was affected under the glycyrrhizic acid concentration of 200 μg/ml. With the glycyrrhizic acid concentration increased to >300 μg/ml, the endothelial cell viability was decreased significantly compared with 0 μg/ml (n = 6; Fig. 13A).

Second, to detect the effect of a noncytotoxic dose of GA (Fig. 13A) on the permeability of ECs (including HUVECs and MAECs), ECs (including HUVEC and MAEC) were cultured with EGM2 medium and GA at concentrations of 50, 100, and 200 μg/ml for 24 h in transwells. The permeability of the endothelial cell (include HUVECs and MAECs) monolayer was detected with Evans blue labeled–BSA. The glycyrrhizic acid at concentrations of 50, 100, and 200 μg/ml could not affect the ECs permeability, including HUVECs and MAECs (Fig. 13B).

Third, we detected weather glycyrrhizic acid at concentrations of 50, 100, and 200 μg/ml could affect the EC permeability (including HUVECs and MAECs) induced by hypoxia trophoblast (including PMTs and JEG-3) CM. HUVECs and MAECs were cultured with 24-h hypoxia JEG3 cells/PMTs CM and GA at concentrations of 50, 100, and 200 μg/ml for 24 h in transwells. Our data showed that glycyrrhizic acid at concentrations of 50, 100, and 200 μg/ml decreased 32.9%, 49.6%, and 89.8%, respective, in the permeability of HUVECs induced by hypoxia JEG-3-CM (Fig. 13C) and decreased 30%, 49.52%, and 88.9%, respectively, in the permeability of MAECs induced by hypoxia PMT-CM (Fig. 13D; n = 6).

In addition, HUVEC permeability induced by hypoxia JEG-3-CM (Fig. 13C) was reversed significantly by 25% with HMGB1 neutralizing Ab (10 μg/ml) compared with control IgG (n = 3; $p <$ 0.05; data not shown).

Discussion

HMGB1 is a 25-kDa, nonhistone, nucleosomal protein (44). In a normal cell, HMGB1 is predominantly localized in the nucleus, where it regulates transcription (45). HMGB1 protein can be released by cells into the extracellular milieu to function as a proinflammatory cytokine in response to injury, infection, and inflammation (46). A variety of factors are reported to induce the release of HMGB1, such as necrosis (47), apoptosis (48), oxida-

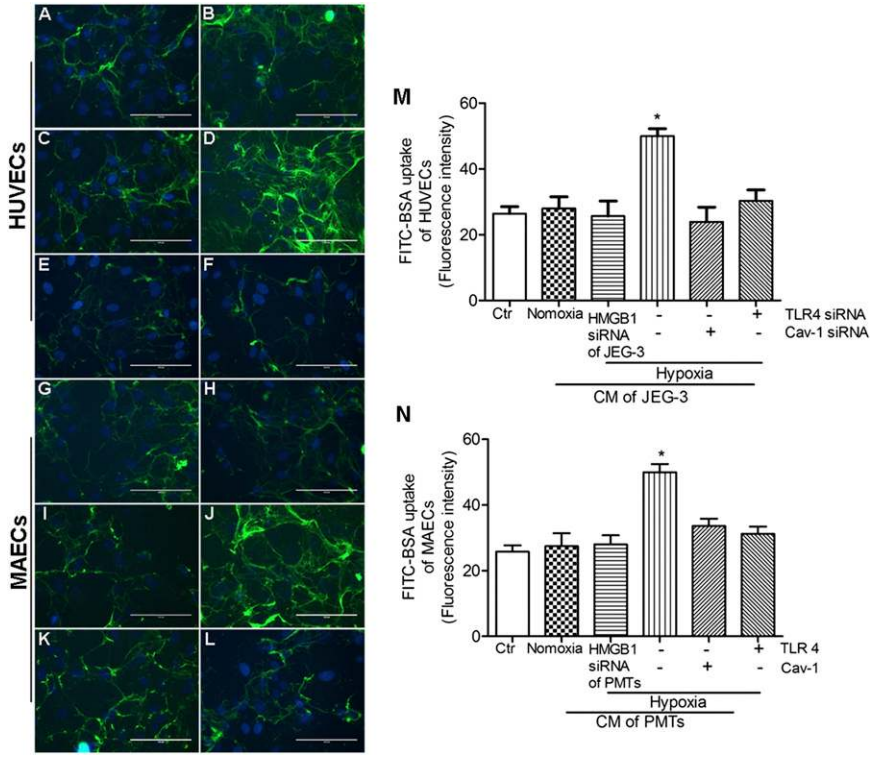

FIGURE 11. Hypoxic trophoblast (include JEG-3 and PMTs) CM increased the FITC-BSA uptake of ECs (include HUVECs and MAECs), which could be reversed by silencing the HMGB1 of trophoblast (include JEG-3 and PMTs) before hypoxia, and also by silencing the TLR4 or CAV-1 in ECs (including HUVECs and MAECs) before incubation with hypoxic trophoblast (including JEG-3 and PMTs) CM. Micrographs (**A**)–(**F**) illustrate FITC-BSA stains of JEG-3 cells with CM-treated HUVECs. (A) HUVECs incubated with EGM-2. (B) Normoxic JEG-3 cells with CM-treated HUVECs. (C) Hypoxic JEG-3 cells with HMGB1-silencing, CM-treated HUVECs. (D) Hypoxic JEG-3 cells with CM-treated HUVECs. (E) Hypoxic JEG-3 cells with CM-treated, TLR4-silencing HUVECs. (F) Hypoxic JEG-3 cells with CM-treated, CAV-1–silencing HUVECs. (**M**) The bar graph shows that the hypoxic JEG-3 CM increased the FITC-BSA uptake (green) of HUVECs, which could be inhibited by TLR4 or CAV-1 silencing of HUVECs. Values were reported as mean ± SD (n = 6). Micrographs (**G**)–(**L**) illustrate FITC-BSA stains of PMT CM-treated MAECs. (G) MAECs incubated with EGM-2. (H) Normoxic JEG-3 cells with CM-treated MAECs. (I) Hypoxic JEG-3 cells with HMGB1-silencing, CM-treated MAECs. (J) Hypoxic PMT CM-treated MAECs. (K) Hypoxic PMT CM-treated TLR4$^{-/-}$ MAECs. (L) Hypoxic PMT CM-treated CAV-1 $^{-/-}$ MAECs. (**N**) The bar graph shows that the hypoxic PMT CM increased the FITC-BSA uptake (green) of MAECs, which could be inhibited by TLR4 or CAV-1 knockout of MAECs. Values were reported as mean ± SD (n = 6). Scale bar, 100μm. *$p < 0.05$, compared with normoxia and control.

tive stress (49), and hypoxia (50), which are all known to be enhanced in the placenta in PE. Trophoblast hypoxia, caused by defective placentation, is a key event in the pathogenesis of PE. Recently, reports have shown that serum HMGB1 levels are increased in severe PE, most notably in patients with early-onset PE (10). In addition, the expression of HMGB1 in the placenta from women with PE was higher than that of women with healthy pregnancies (51).

In the present experiments, we found that HMGB1 was detected in JEG-3 cells and PMT culture media of 1% oxygen and the amount of HMGB1 protein increased significantly after 24 h of incubation compared with normoxia. HMGB1 protein and gene expression of hypoxic trophoblasts, including JEG-3 cells and PMTs, were also significantly increased compared with normoxic (21% oxygen) JEG-3 cells and PMTs. JEG-3 cells and PMTs viability decreased significantly after 24 h of hypoxia, and at the same time JC1 and Hoechst staining showed that 24 h of hypoxia decreased the mitochondrial membrane potential (indicating early cell apoptosis) and increased trophoblast cell (including JEG-3 cells and PMTs) apoptosis. These data suggest that oxidative stress or trophoblast apoptosis release the damage-associated molecular pattern HMGB1 into the extracellular milieu actively or passively. HMGB1 could play an important role in trophoblast oxidative stress–associated pregnancy conditions, such as PE and fetal growth restriction.

Besides regulating the transcriptional procession and transduction of the innate immune system via its damage function during tissue hypoxia, injury, and infection, HMGB1 has also been described to influence endothelial cell function, such as cytoskeletal rearrangement, to upregulate adhesion molecules and to increase cell permeability (7). To detect whether increased HMGB1 in hypoxic trophoblast CM affects the permeability of endothelial cells, we applied hypoxic trophoblast CM to the endothelial cell monolayer. Our data showed that after 24 h of incubation, 24-h hypoxic trophoblast CM increased endothelial cell monolayer permeability compared with normoxic trophoblast CM, and the increased permeability was reversed by trophoblasts HMGB1 siRNA transfection before hypoxia. GA, the main component of radix glycyrrhizae, has a variety of pharmacologic activities (19–22). Recent studies showed that GA played an important role in the inhibition of HMGB1 (23, 24). Our data showed that GA at the concentration of 200 μg/ml decreased by 89.8% in the permeability of HUVECs induced by hypoxia JEG-3–CM, and decreased by 88.9% in the permeability of MAECs induced by hypoxia PMT-CM, respectively. In addition, HMGB1 neutralizing Ab at 10 μg/ml decreased by 25% in the permeability of HUVECs induced by hypoxia JEG-3–CM. Consistent with a previous report by Huang et al. (52), HMGB1 increased the endothelial cell monolayer permeability. Our data indicate that the hypoxic trophoblasts in PE could release damage-associated molecular

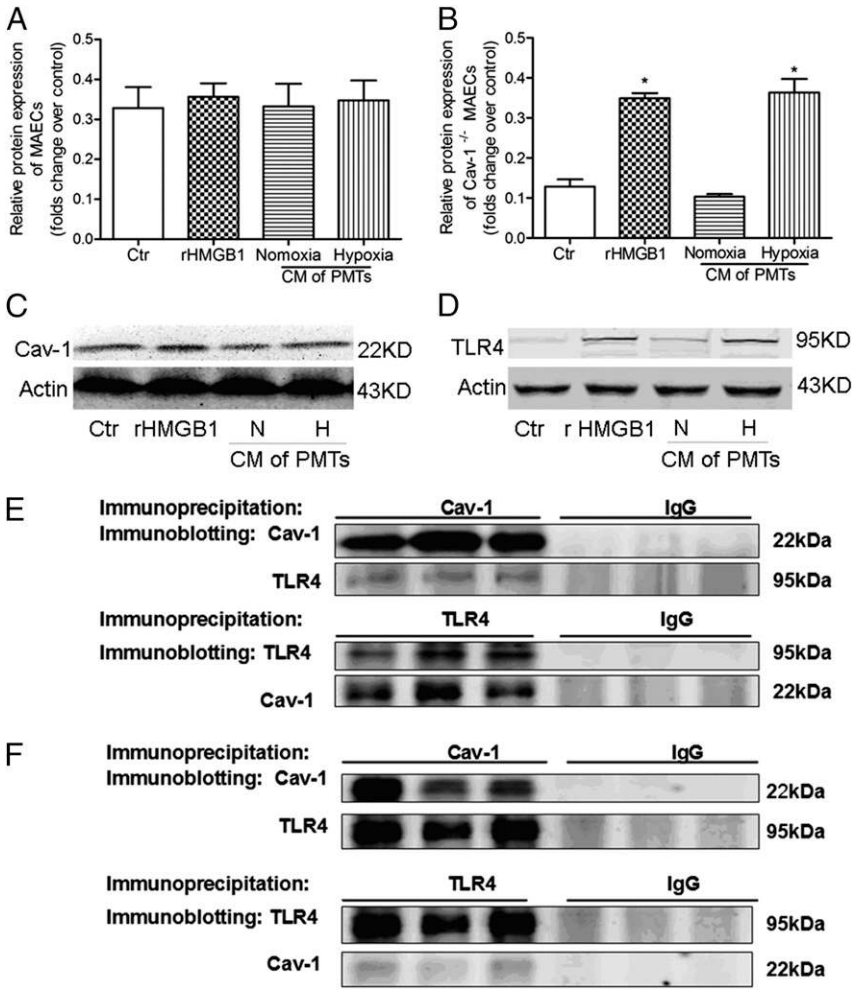

FIGURE 12. The relationship between TLR4 and CAV-1 in HUVECs and MAECs and the colocalization of CAV-1 and TLR4 in the protein of HUVECs and C57BL/6 mouse kidney by coimmunoprecipitation analysis. (**A** and **C**) Representative Western blot showing CAV-1 protein expression in TLR4$^{-/-}$ MAECs incubated with 24 h normoxic PMT CM, hypoxic PMT CM, and EGM-2 medium with rHMGB1 (1 μg/ml) incubated for 24 h. Values are reported as mean ± SD (n = 6). (**B** and **D**) Representative Western blot showing TLR4 protein expression in CAV1$^{-/-}$ MAECs incubated with 24-h normoxic PMT CM, hypoxic PMT CM, and EGM-2 medium with rHMGB1 (1 μg/ml) incubated for 24 h. Values are reported as mean ± SD (n = 6). (**E** and **F**) Representative coimmunoprecipitation analysis of colocalization of CAV-1 and TLR4 in (E) HUVECs and (F) C57BL/6 mouse kidney (n = 3). *$p < 0.05$, compared with normoxia and control. Ctr, endothelial cells incubated with EGM-2; H, hypoxia; N, normoxia.

patterns (HMGB1), further enhancing vascular endothelial permeability, which can play a key role in the clinical features, including general edema and urine protein.

Recent studies showed that caveolae play an important role in the transcellular transport of serum protein in physiologic and pathologic processes (13–15). CAV-1 is the main structural component of endothelial caveolae and regulates endothelial transcytosis. Recent studies have shown that CAV-1 plays a key role in the regulation of microvascular endothelial and blood-retinal barrier permeability (42, 53). Our results showed that CM from hypoxic trophoblast and HMGB1 increased endothelial cell monolayer permeability and increased CAV-1 protein expression at the same time. The cultured, CAV-1–deficient endothelial cells (CAV-1$^{-/-}$-MAECs or CAV-1 siRNA) reversed the increasing permeability stimulated by hypoxic trophoblast (JEG-3 cell and PMT) CM. Our data suggest that HMGB1 released from hypoxic trophoblasts increased endothelial cell monolayer permeability in a CAV-1–dependent manner.

Inflammatory stimuli could increase paracellular transport by causing gaps in intercellular adherens junctions. VE-cadherin is the main component of intercellular adherent junctions (54, 55). Phosphorylation of VE-cadherins at the plasma membrane could increase paracellular leaks (56, 57) and endocytosis (54, 58) in cultured endothelial cells. However, our in vitro experiments failed to find the alteration of endothelial cell VE-cadherin and phosphorylated VE-cadherin following treatment of hypoxic trophoblast (including JEG-3 cell and PMT) CM (immunoblotting; data not shown), suggesting the existence of an independent pathway.

TLR4 is one of the principal signal-transducing receptors for HMGB1. Our data showed that hypoxic trophoblast CM increased the TLR4 protein expression and endothelial cell monolayer permeability at the same time. Again, pretreating HUVECs with TLR4 siRNA reversed the hypoxic JEG-3 cell CM dependence, increasing the permeability of the HUVEC monolayer. These stimulatory effects of hypoxic PMT CM on MAEC permeability and albumin endocytosis were abolished in TLR4-deficient MAECs, corroborating the notion that increased HMGB1 in hypoxic trophoblast CM increased the permeability of the endothelial cell monolayer via the TLR4 pathway.

The recruitment of TLR4 into lipid rafts has been observed upon LPS stimulation (59). Ethanol triggered the internalization and intracellular trafficking of IL-1RI and TLR4 via caveolar-dependent endocytosis in astrocytes (60). CAV-1 is thought to play a central role in signal regulation within the caveolae through direct regulatory interactions with TLR4 (61). Our experiment shows that hypoxic trophoblast CM and HMGB1 increase the permeability of the endothelial cell monolayer and TLR4 in parallel with elevated CAV-1 protein expression in endothelial cells. TLR4 and CAV-1 may act together on the hypoxic trophoblast-induced permeability of the endothelial cell monolayer. Our data showed that hypoxic trophoblast CM and HMGB1 increase the TLR4 protein expression of CAV-1–silencing endothelial cells, but did not increase the CAV-1 protein expression in TLR4-silencing

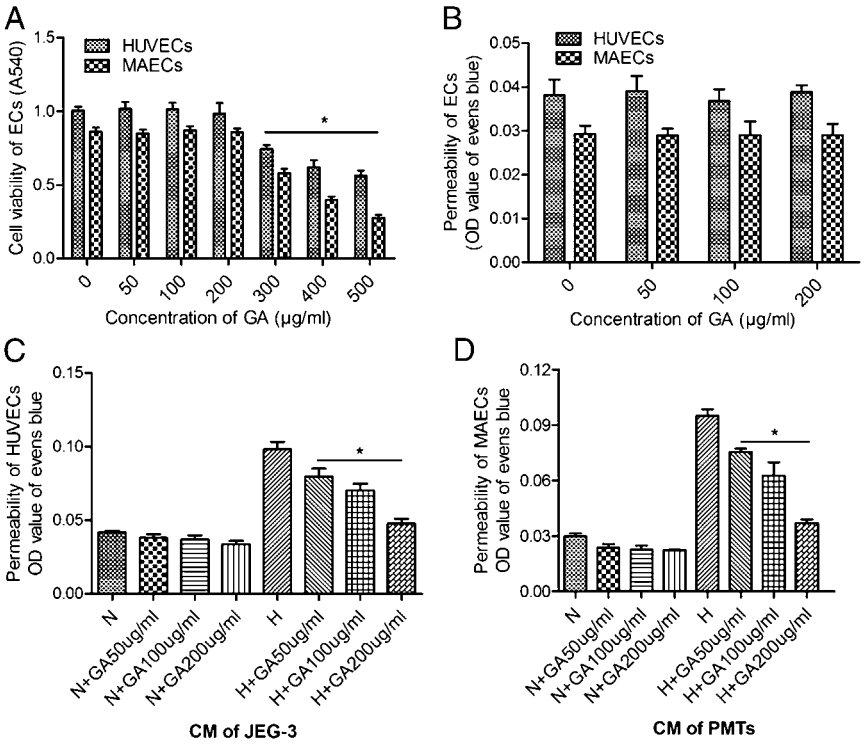

FIGURE 13. The effect of glycyrrhizic acid on the permeability of the endothelial cell (HUVECs and MAECs) monolayer induced by hypoxia trophoblast (including PMTs and JEG-3) CM. (**A**) Cytotoxic dose of GA on ECs (including HUVECs and MAECs). ECs (including HUVEC and MAEC) were cultured with EGM2 medium and GA at concentrations ranging from 50 to 500 μg/ml for 24 h. The cell viability was detected with the MTT method. Values are reported as mean ± SD (n = 6). *$p < 0.05$, compared with 0 μg/ml. (**B**) The effect of noncytotoxic dose of GA on the permeability of ECs (including HUVECs and MAECs). ECs (including HUVECs and MAECs) were cultured with EGM2 medium and GA at concentrations of 50, 100, and 200 for 24 h in transwells. The permeability of the endothelial cell (including HUVECs and MAECs) monolayer was detected with Evans blue–labeled BSA (n = 6). (**C** and **D**) We detected whether glycyrrhizic acid at concentrations of 50, 100, and 200 μg/ml could affect the EC permeability (including HUVECs and MAECs) induced by hypoxia trophoblast (including PMT and JEG-3) CM. Values are reported as mean ± SD (n = 6). *$p < 0.05$, compared with hypoxia. H, hypoxia; N, normoxia.

endothelial cells. These results suggest that CAV-1 is a subpathway of the HMGB1-TLR4 pathway. To detect whether CAV-1 and TLR4 are colocalized in HUVECs, we used immunofluorescence analysis and immunoprecipitation to test the colocalization of CAV-1 and TLR4 in HUVECs. Our data showed that CAV-1 and TLR4 are colocalized in HUVECs. Our data also showed the colocalization of TLR4 and CAV-1 in C57BL/6 mouse kidney. These data suggest that the recruitment of TLR4 into lipid rafts and its colocalization with CAV-1 play an important role in the HMGB1-induced permeability of HUVECs.

TLR2 and RAGE are the principal signal-transducing HMGB1 receptors (11, 12), but our data showed that hypoxic trophoblast CM and rHMGB1 at the concentration of 1 μg/ml did not increase TLR2 and RAGE protein expression of endothelial cells. These data suggested that the hypoxic trophoblast-induced permeability of the endothelial cell monolayer is independent of TLR2 and RAGE.

Placental hypoxia, which is the main pathologic feature of PE, can cause trophoblast hypoxia, necrosis, and apoptosis (8, 9). HMGB1 released actively or passively by hypoxia trophoblast increased the permeability of endothelial cell monolayer by TLR4–CAV-1 pathway. High endothelial cell permeability is the mean cause of general edema and high urine protein in PE. General edema and high urine protein are the main characteristics of PE (8). Our data showed that hypoxia trophoblast HMGB1 could play an important role on the clinical characteristics including general edema and high urine protein. Inhibiting the activation of HMGB1-TLR4–CAV-1 pathway could provide an especially promising drug target for people with PE.

The limitations of this study are that our work was just conducted using cells in culture and an in vitro hypoxia model. The JEG-3 cell line did not display all the physiologic characteristics of human placental trophoblasts. The permeability of the aortic endothelium or HUVECs is arguably not a good model for the vasculature of the kidney or the glomerulus. We will explore the role of hypoxic trophoblast on the permeability of glomerular filtration membrane (coculture of glomerular endothelial cells and podocyte cell line) in an in vitro model. In addition, we will explore the role of the HMGB1/TLR4/CAV-1 pathway in the permeability of the glomerular filtration membrane in a mouse PE model.

Acknowledgments

We thank Dr. Timothy Billiar and his colleagues from the Department of Surgery at the University of Pittsburgh School of Medicine for support and Dr. Kevin Tracey (North Shore-LIJ Health System Feinstein Institute for Medical Research) for the HMGB1 neutralizing Ab.

Disclosures

The authors have no financial conflicts of interest.

References

1. Bauer, E. M., R. Shapiro, H. Zheng, F. Ahmad, D. Ishizawar, S. A. Comhair, S. C. Erzurum, T. R. Billiar, and P. M. Bauer. 2012. High mobility group box 1 contributes to the pathogenesis of experimental pulmonary hypertension via activation of Toll-like receptor 4. *Mol. Med.* 18: 1509–1518.
2. Lotze, M. T., and R. A. DeMarco. 2003. Dealing with death: HMGB1 as a novel target for cancer therapy. *Curr. Opin. Investig. Drugs* 4: 1405–1409.
3. Krysko, D. V., A. D. Garg, A. Kaczmarek, O. Krysko, P. Agostinis, and P. Vandenabeele. 2012. Immunogenic cell death and DAMPs in cancer therapy. *Nat. Rev. Cancer* 12: 860–875.
4. Tang, D., R. Kang, H. J. Zeh, III, and M. T. Lotze. 2011. High-mobility group box 1, oxidative stress, and disease. *Antioxid. Redox Signal.* 14: 1315–1335.
5. Lei, C., S. Lin, C. Zhang, W. Tao, W. Dong, Z. Hao, M. Liu, and B. Wu. 2013. Effects of high-mobility group box1 on cerebral angiogenesis and neurogenesis after intracerebral hemorrhage. *Neuroscience* 229: 12–19.
6. Zhang, J., H. K. Takahashi, K. Liu, H. Wake, R. Liu, T. Maruo, I. Date, T. Yoshino, A. Ohtsuka, S. Mori, and M. Nishibori. 2011. Anti-high mobility group box-1 monoclonal antibody protects the blood-brain barrier from ischemia-induced disruption in rats. *Stroke* 42: 1420–1428.
7. Wolfson, R. K., E. T. Chiang, and J. G. Garcia. 2011. HMGB1 induces human lung endothelial cell cytoskeletal rearrangement and barrier disruption. *Microvasc. Res.* 81: 189–197.
8. Lee, S. M., R. Romero, Y. J. Lee, I. S. Park, C. W. Park, and B. H. Yoon. 2012. Systemic inflammatory stimulation by microparticles derived from hypoxic trophoblast as a model for inflammatory response in preeclampsia. *Am. J. Obstet. Gynecol.* 207: 337.e1–337.e8.
9. Chen, B., M. S. Longtine, and D. M. Nelson. 2012. Hypoxia induces autophagy in primary human trophoblasts. *Endocrinology* 153: 4946–4954.
10. Naruse, K., T. Sado, T. Noguchi, T. Tsunemi, S. Yoshida, J. Akasaka, N. Koike, H. Oi, and H. Kobayashi. 2012. Peripheral RAGE (receptor for advanced glycation endproducts)-ligands in normal pregnancy and preeclampsia: novel markers of inflammatory response. *J. Reprod. Immunol.* 93: 69–74.

11. Tafani, M., L. Schito, L. Pellegrini, L. Villanova, G. Marfe, T. Anwar, R. Rosa, M. Indelicato, M. Fini, B. Pucci, and M. A. Russo. 2011. Hypoxia-increased RAGE and P2X7R expression regulates tumor cell invasion through phosphorylation of Erk1/2 and Akt and nuclear translocation of NF-kappaB. *Carcinogenesis* 32: 1167–1175.
12. Cohen, M. J., M. Carles, K. Brohi, C. S. Calfee, P. Rahn, M. S. Call, B. B. Chesebro, M. A. West, and J. F. Pittet. 2010. Early release of soluble receptor for advanced glycation endproducts after severe trauma in humans. *J. Trauma* 68: 1273–1278.
13. Orsenigo, F., C. Giampietro, A. Ferrari, M. Corada, A. Galaup, S. Sigismund, G. Ristagno, L. Maddaluno, G. Y. Koh, D. Franco, et al. 2012. Phosphorylation of VE-cadherin is modulated by haemodynamic forces and contributes to the regulation of vascular permeability in vivo. *Nat. Commun.* 3: 1208.
14. Sun, Y., G. Hu, X. Zhang, and R. D. Minshall. 2009. Phosphorylation of caveolin-1 regulates oxidant-induced pulmonary vascular permeability via paracellular and transcellular pathways. *Circ. Res.* 105: 676–685, 15, 685.
15. Siddiqui, M. R., Y. A. Komarova, S. M. Vogel, X. Gao, M. G. Bonini, J. Rajasingh, Y. Y. Zhao, V. Brovkovych, and A. B. Malik. 2011. Caveolin-1-eNOS signaling promotes p190RhoGAP-A nitration and endothelial permeability. *J. Cell Biol.* 193: 841–850.
16. Wang, F., X. Song, M. Zhou, L. Wei, Q. Dai, Z. Li, N. Lu, and Q. Guo. 2013. Wogonin inhibits H2O2-induced vascular permeability through suppressing the phosphorylation of caveolin-1. *Toxicology* 305: 10–19.
17. Thomas, C. P., J. I. Andrews, N. S. Raikwar, E. A. Kelley, F. Herse, R. Dechend, T. G. Golos, and K. Z. Liu. 2009. A recently evolved novel trophoblast-enriched secreted form of fms-like tyrosine kinase-1 variant is up-regulated in hypoxia and preeclampsia. *J. Clin. Endocrinol. Metab.* 94: 2524–2530.
18. Hannan, N. J., P. Paiva, E. Dimitriadis, and L. A. Salamonsen. 2010. Models for study of human embryo implantation: choice of cell lines? *Biol. Reprod.* 82: 235–245.
19. Isbrucker, R. A., and G. A. Burdock. 2006. Risk and safety assessment on the consumption of Licorice root (Glycyrrhiza sp.), its extract and powder as a food ingredient, with emphasis on the pharmacology and toxicology of glycyrrhizin. *Regul. Toxicol. Pharmacol.* 46: 167–192.
20. Hennell, J. R., S. Lee, C. S. Khoo, M. J. Gray, and A. Bensoussan. 2008. The determination of glycyrrhizic acid in Glycyrrhiza uralensis Fisch. ex DC. (Zhi Gan Cao) root and the dried aqueous extract by LC-DAD. *J. Pharm. Biomed. Anal.* 47: 494–500.
21. Kimura, M., T. Moro, H. Motegi, H. Maruyama, M. Sekine, H. Okamoto, H. Inoue, T. Sato, and M. Ogihara. 2008. In vivo glycyrrhizin accelerates liver regeneration and rapidly lowers serum transaminase activities in 70% partially hepatectomized rats. *Eur. J. Pharmacol.* 579: 357–364.
22. Kurisu, S., I. Inoue, T. Kawagoe, M. Ishihara, Y. Shimatani, Y. Nakama, T. Maruhashi, E. Kagawa, K. Dai, T. Aokage, et al. 2008. Clinical profile of patients with symptomatic glycyrrhizin-induced hypokalemia. *J. Am. Geriatr. Soc.* 56: 1579–1581.
23. Ogiku, M., H. Kono, M. Hara, M. Tsuchiya, and H. Fujii. 2011. Glycyrrhizin prevents liver injury by inhibition of high-mobility group box 1 production by Kupffer cells after ischemia-reperfusion in rats. *J. Pharmacol. Exp. Ther.* 339: 93–98.
24. Yamaguchi, H., Y. Kidachi, K. Kamiie, T. Noshita, and H. Umetsu. 2012. Structural insight into the ligand-receptor interaction between glycyrrhetinic acid (GA) and the high-mobility group protein B1 (HMGB1)-DNA complex. *Bioinformation* 8: 1147–1153.
25. Ohhata, T., C. E. Senner, M. Hemberger, and A. Wutz. 2011. Lineage-specific function of the noncoding Tsix RNA for Xist repression and Xi reactivation in mice. *Genes Dev.* 25: 1702–1715.
26. Schulz, L. C., and E. P. Widmaier. 2004. The effect of leptin on mouse trophoblast cell invasion. *Biol. Reprod.* 71: 1963–1967.
27. Wang, X. H., S. F. Chen, H. M. Jin, and R. M. Hu. 2009. Differential analyses of angiogenesis and expression of growth factors in micro- and macrovascular endothelial cells of type 2 diabetic rats. *Life Sci.* 84: 240–249.
28. Tadie, J. M., H. B. Bae, J. S. Deshane, C. P. Bell, E. R. Lazarowski, D. D. Chaplin, V. J. Thannickal, E. Abraham, and J. W. Zmijewski. 2012. Toll-like receptor 4 engagement inhibits adenosine 5′-monophosphate-activated protein kinase activation through a high mobility group box 1 protein-dependent mechanism. *Mol. Med.* 18: 659–668.
29. Yedwab, G. A., G. Paz, T. Z. Homonnai, M. P. David, and P. F. Kraicer. 1976. The temperature, pH, and partial pressure of oxygen in the cervix and uterus of women and uterus of rats during the cycle. *Fertil. Steril.* 27: 304–309.
30. Ottosen, L. D., J. Hindkaer, M. Husth, D. E. Petersen, J. Kirk, and H. J. Ingerslev. 2006. Observations on intrauterine oxygen tension measured by fibre-optic microsensors. *Reprod. Biomed. Online* 13: 380–385.
31. Heazell, A. E., S. J. Moll, C. J. Jones, P. N. Baker, and I. P. Crocker. 2007. Formation of syncytial knots is increased by hyperoxia, hypoxia and reactive oxygen species. *Placenta.* 28(Suppl. A): S33–S40.
32. Zhou, C. C., S. Ahmad, T. Mi, S. Abbasi, L. Xia, M. C. Day, S. M. Ramin, A. Ahmed, R. E. Kellems, and Y. Xia. 2008. Autoantibody from women with preeclampsia induces soluble Fms-like tyrosine kinase-1 production via angiotensin type 1 receptor and calcineurin/nuclear factor of activated T-cells signaling. *Hypertension* 51: 1010–1019.
33. Edelman, D. A., Y. Jiang, J. G. Tyburski, R. F. Wilson, and C. P. Steffes. 2007. Lipopolysaccharide activation of pericyte's Toll-like receptor-4 regulates coculture permeability. *Am. J. Surg.* 193: 730–735.
34. Liu, J., X. Jin, K. J. Liu, and W. Liu. 2012. Matrix metalloproteinase-2-mediated occludin degradation and caveolin-1-mediated claudin-5 redistribution contribute to blood-brain barrier damage in early ischemic stroke stage. *J. Neurosci.* 32: 3044–3057.
35. Ge, W. S., J. X. Wu, J. G. Fan, Y. J. Wang, and Y. W. Chen. 2011. Inhibition of high-mobility group box 1 expression by siRNA in rat hepatic stellate cells. *World J. Gastroenterol.* 17: 4090–4098.
36. Brenner, M. P., C. Silva-Frade, M. C. Ferrarezi, A. F. Garcia, E. F. Flores, and T. C. Cardoso. 2012. Evaluation of developmental changes in bovine in vitro produced embryos following exposure to bovine Herpesvirus type 5. *Reprod. Biol. Endocrinol.* 10: 53.
37. Spinnler, R., T. Gorski, K. Stolz, S. Schuster, A. Garten, A. G. Beck-Sickinger, M. A. Engelse, E. J. de Koning, A. Körner, W. Kiess, and K. Maedler. 2013. The adipocytokine Nampt and its product NMN have no effect on beta-cell survival but potentiate glucose stimulated insulin secretion. *PLoS ONE* 8: e54106.
38. Zhang, B., Q. Wu, X. F. Ye, S. Liu, X. F. Lin, and M. C. Chen. 2003. Roles of PLC-gamma2 and PKCalpha in TPA-induced apoptosis of gastric cancer cells. *World J. Gastroenterol.* 9: 2413–2418.
39. Kalff, J. C., A. Türler, N. T. Schwarz, W. H. Schraut, K. K. Lee, D. J. Tweardy, T. R. Billiar, R. L. Simmons, and A. J. Bauer. 2003. Intra-abdominal activation of a local inflammatory response within the human muscularis externa during laparotomy. *Ann. Surg.* 237: 301–315.
40. Du, Y. H., Y. Y. Guan, N. J. Alp, K. M. Channon, and A. F. Chen. 2008. Endothelium-specific GTP cyclohydrolase I overexpression attenuates blood pressure progression in salt-sensitive low-renin hypertension. *Circulation* 117: 1045–1054.
41. Lee, W., T. H. Kim, S. K. Ku, K. J. Min, H. S. Lee, T. K. Kwon, and J. S. Bae. 2012. Barrier protective effects of withaferin A in HMGB1-induced inflammatory responses in both cellular and animal models. *Toxicol. Appl. Pharmacol.* 262: 91–98.
42. Chen, W., B. Gassner, S. Börner, V. O. Nikolaev, N. Schlegel, J. Waschke, N. Steinbronn, R. Strasser, and M. Kuhn. 2012. Atrial natriuretic peptide enhances microvascular albumin permeability by the caveolae-mediated transcellular pathway. *Cardiovasc. Res.* 93: 141–151.
43. Lee, I. T., R. H. Shih, C. C. Lin, J. T. Chen, and C. M. Yang. 2012. Role of TLR4/NADPH oxidase/ROS-activated p38 MAPK in VCAM-1 expression induced by lipopolysaccharide in human renal mesangial cells. *Cell Commun. Signal.* 10: 33.
44. Bianchi, M. E., and A. A. Manfredi. 2007. High-mobility group box 1 (HMGB1) protein at the crossroads between innate and adaptive immunity. *Immunol. Rev.* 220: 35–46.
45. Ge, H., and R. G. Roeder. 1994. The high mobility group protein HMG1 can reversibly inhibit class II gene transcription by interaction with the TATA-binding protein. *J. Biol. Chem.* 269: 17136–17140.
46. Yang, H., H. Wang, C. J. Czura, and K. J. Tracey. 2005. The cytokine activity of HMGB1. *J. Leukoc. Biol.* 78: 1–8.
47. Scaffidi, P., T. Misteli, and M. E. Bianchi. 2002. Release of chromatin protein HMGB1 by necrotic cells triggers inflammation. *Nature* 418: 191–195.
48. Gauley, J., and D. S. Pisetsky. 2009. The translocation of HMGB1 during cell activation and cell death. *Autoimmunity* 42: 299–301.
49. Tsung, A., J. R. Klune, X. Zhang, G. Jeyabalan, Z. Cao, X. Peng, D. B. Stolz, D. A. Geller, M. R. Rosengart, and T. R. Billiar. 2007. HMGB1 release induced by liver ischemia involves Toll-like receptor 4 dependent reactive oxygen species production and calcium-mediated signaling. *J. Exp. Med.* 204: 2913–2923.
50. Hamada, T., M. Torikai, A. Kuwazuru, M. Tanaka, N. Horai, T. Fukuda, S. Yamada, S. Nagayama, K. Hashiguchi, N. Sunahara, et al. 2008. Extracellular high mobility group box chromosomal protein 1 is a coupling factor for hypoxia and inflammation in arthritis. *Arthritis Rheum.* 58: 2675–2685.
51. Wang, B., K. Koga, Y. Osuga, T. Hirata, A. Saito, O. Yoshino, Y. Hirota, M. Harada, Y. Takemura, T. Fujii, and Y. Taketani. 2011. High mobility group box 1 (HMGB1) levels in the placenta and in serum in preeclampsia. *Am. J. Reprod. Immunol.* 66: 143–148.
52. Wang, Y., D. F. Lewis, J. S. Alexander, and D. N. Granger. 2007. Endothelial barrier function in preeclampsia. *Front. Biosci.* 12: 2412e24.
53. Tian, X. F., X. B. Xia, H. Z. Xu, S. Q. Xiong, and J. Jiang. 2012. Caveolin-1 expression regulates blood-retinal barrier permeability and retinal neovascularization in oxygen-induced retinopathy. *Clin. Experiment. Ophthalmol.* 40: e58–e66.
54. Dejana, E., F. Orsenigo, and M. G. Lampugnani. 2008. The role of adherens junctions and VE-cadherin in the control of vascular permeability. *J. Cell Sci.* 121: 2115–2122.
55. Esser, S., M. G. Lampugnani, M. Corada, E. Dejana, and W. Risau. 1998. Vascular endothelial growth factor induces VE-cadherin tyrosine phosphorylation in endothelial cells. *J. Cell Sci.* 111: 1853–1865.
56. Gorbunova, E. E., I. N. Gavrilovskaya, T. Pepini, and E. R. Mackow. 2011. VEGFR2 and Src kinase inhibitors suppress Andes virus-induced endothelial cell permeability. *J. Virol.* 85: 2296–2303.
57. Navarro, P., L. Caveda, F. Breviario, I. Mândoteanu, M. G. Lampugnani, and E. Dejana. 1995. Catenin-dependent and -independent functions of vascular endothelial cadherin. *J. Biol. Chem.* 270: 30965–30972.
58. Hou, W. H., I. H. Liu, C. C. Tsai, F. E. Johnson, S. S. Huang, and J. S. Huang. 2011. CRSBP-1/LYVE-1 ligands disrupt lymphatic intercellular adhesion by inducing tyrosine phosphorylation and internalization of VE-cadherin. *J. Cell Sci.* 124: 1231–1244.
59. Zou, J., D. Feng, W. H. Ling, and R. D. Duan. 2013. Lycopene suppresses proinflammatory response in lipopolysaccharide-stimulated macrophages by inhibiting ROS-induced trafficking of TLR4 to lipid raft-like domains. *J. Nutr. Biochem.* 24: 1117–1122.
60. Blanco, A. M., A. Perez-Arago, S. Fernandez-Lizarbe, and C. Guerri. 2008. Ethanol mimics ligand-mediated activation and endocytosis of IL-1RI/TLR4 receptors via lipid rafts caveolae in astroglial cells. *J. Neurochem.* 106: 625–639.
61. Wang, X. M., H. P. Kim, K. Nakahira, S. W. Ryter, and A. M. Choi. 2009. The heme oxygenase-1/carbon monoxide pathway suppresses TLR4 signaling by regulating the interaction of TLR4 with caveolin-1. *J. Immunol.* 182: 3809–3818.